論文 / 著書情報
Article / Book Information

題目(和文)	核不安定モデルに基づいた木星型惑星のガス集積過程
Title(English)	The Gas Accretion Process of Giant Planets on the Basis of the Nucleated Instability Model
著者(和文)	生駒大洋
Author(English)	Masahiro Ikoma
出典(和文)	学位:理学博士, 学位授与機関:東京工業大学, 報告番号:甲第4623号, 授与年月日:2001年3月26日, 学位の種別:課程博士, 審査員:中沢清
Citation(English)	Degree:Doctor of Science, Conferring organization: Tokyo Institute of Technology, Report number:甲第4623号, Conferred date:2001/3/26, Degree Type:Course doctor, Examiner:
学位種別(和文)	博士論文
Type(English)	Doctoral Thesis

The Gas Accretion Process of Giant Planets on the Basis of the Nucleated Instability Model

MASAHIRO IKOMA

Department of Earth and Planetary Sciences

Graduate School of Science and Engineering

Tokyo Institute of Technology

Doctoral Thesis

March 2001

Abstract

The giant planets (i.e., Jupiter-like planets) are characterized by massive hydrogen-rich atmospheres (which are often called *envelopes*). The formation of the envelopes is explained in the context of the nucleated instability model. According to this model, when an ice-rich core, which is embedded in a hydrogen-rich nebula, grows to a critical mass owing to planetesimal accretion, it captures the surrounding nebular gas to form a massive envelope. The widely accepted value of the critical core mass, more than about $10M_\oplus$ ($M_\oplus$: Earth mass), was based on some nominal values of the parameters involved in this model. This value is, however, larger than the estimated mass of the core of Jupiter ($< 10M_\oplus$) and seems to be too large to be formed within the lifetime of the nebula ($\sim 10^7$yr). Furthermore, the existence of the extrasolar giant planets orbiting very close to their central stars implies that the critical core mass should be smaller than $10M_\oplus$, because there would be insufficient mass of solid materials around their present locations to produce such massive cores.

The accretion of the envelope is regulated by core accretion rate and grain opacity. According to the planetary accretion theory, the core accretion rate varies considerably, depending on the stage of planetary growth. In particular, it is suggested that the core accretion would almost stop before the mass of the core reaches the conventional critical core mass. The previous works cannot give any answer to how the gas accretion proceeds after the core accretion has stopped. The grain opacity of the ancient envelope gas is highly uncertain, because it depends on the abundance and sizes of the grains that are quite difficult to know. Furthermore, to explain the formation of a variety of the extrasolar giant planets, we should take difference in the physical properties of the planet-forming nebulae into consideration. In this study, we have investigated the accretion time of the envelope as well as the critical core mass for a wide range of the core accretion rate, the grain opacity, and the density and temperature of the nebular gas. We have also studied the case in which the core accretion stops before the onset of rapid gas accretion.

Our main results are as follows. (1) The critical core mass is as small as $\sim 0.1M_\oplus$ for sufficiently small core accretion rate and/or grain opacity, which indicates even a small core ($\gtrsim 0.1M_\oplus$) can begin to capture the nebular gas, if its growth stops. (2) The accretion time of the envelope, $\tau_{\rm g}$, depends strongly on the critical core mass, moderately on the grain opacity, and very weakly on the past core accretion process; $\tau_{\rm g}$ is expressed approximately as $\tau_{\rm g} \sim 1 \times 10^{10} f (M_{\rm c}/M_\oplus)^{-3.5}$yr, where $M_{\rm c}$ is the critical core mass and f is the ratio of the grain opacity in the envelope to that in the interstellar cloud. (3) The critical core mass (and the accretion time of the envelope) decreases with increasing nebular density and decreasing nebular temperature. Furthermore, the critical core mass decreases as the distance from the central star decreases in typical nebula models; for example, it reduces to $2-3M_\oplus$ at 0.05AU in a dense nebula with surface density about 10 times as large as that of the minimum-mass solar nebula.

Our results combined with those of the planetary accretion theory suggest the following. Jupiter could form at its current position within a few 10^7yr, if $f \leq 0.01$ or the initial surface density of solid materials, $\Sigma_{\rm d}$, was a few times larger than that of the minimum-mass solar nebula, $\Sigma_{\rm d}^{\rm H}$. Furthermore, the mass of the core at the onset time of the gas accretion would be 2 to $9M_\oplus$, which is consistent with the present core mass of Jupiter ($< 10M_\oplus$). On the other hand, the extrasolar giant planets orbiting around 0.05AU could form in their current positions in a period much shorter than 1×10^7yr if $\Sigma_{\rm d} \sim 10\Sigma_{\rm d}^{\rm H}$; such nebulae have been detected observationally. For Saturn, Uranus, and Neptune, gravitational effects of Jupiter, which formed earlier than they, should be considered (for example, outward migration of protoplanets). In considering such special conditions, our results are useful and can be readily applied to the problems.

Contents

1 Introduction

From the physical point of view, planets are classified in two major categories: the terrestrial planets and the giant planets. In the solar system, Mercury, Venus, the Earth, and Mars belong to the former and Jupiter, Saturn, Uranus, and Neptune to the latter. Roughly speaking, the giant planets have three different physical properties from those of the terrestrial planets. First, the giant planets have large masses of 8.68×10^{28}g (Uranus) to 1.90×10^{30}g (Jupiter), whereas the mass of the largest terrestrial planet, the Earth, is 5.98×10^{27}g. Next, the giant planets have a large amount of hydrogen and helium; by contrast, the terrestrial planets are mainly composed of rocky and metallic materials. Finally, while the terrestrial planets exist in the inner parts of the solar system, from 0.39 (Mercury) to 1.52 AU (Mars) (AU is the astronomical unit of distance and equal to the semimajor axis of the Earth, 1.5×10^{13}cm), the giant planets exist in the outer region, from 5.20 (Jupiter) to 30.1 AU (Neptune). It is an interesting issue why the solar system has two kinds of planets.

The recent observations of Keplerian Doppler shifts in solar-type stars have revealed that there exist planetary systems other than the solar system (see Marcy and Butler (1998) for a review). To date, about 50 planets have been detected, since the first discovery of 51 Peg b by Mayor and Queloz (1995). All of them are comparable in mass to Jupiter. These planets are called extrasolar planets. What is surprising is that, whereas our giant planets exist in the outer parts of the solar system, the extrasolar planets have orbits with very small semimajor axes (from 0.05 to 3 AU). Thus, we are faced with another intriguing problem, which is how the planetary systems

apparently different from our solar system were formed.

1.1 Formation Processes of the Giant Planets

The formation of the giant planets can be explained within the scenario of *the nucleated instability model*, which is predicted by the standard theory of planetary formation (Safronov 1969; Hayashi *et al.* 1985). According to the standard theory, there exists a centrifugally supported, flattened disk composed of gas and dust (which is hereafter called a nebula) around a young central star at the starting point of planetary formation. In the nebula, planetesimals with sizes of the order of a kilometer are formed through gravitational fragmentation of a sedimentary dust-layer (Goldreich and Ward 1973; Sekiya 1983) or through direct sticking of μm-size particles (Weidenschilling 1980; Cuzzi *et al.* 1993). Then, a number of planetesimals collide and coalesce with each other to form relatively massive protoplanets. When the protoplanet embedded in the nebula grows in mass to about the lunar mass ($\sim 1 \times 10^{25}$g), it can attract the surrounding nebular gas gravitationally, although the mass of the attracted gas is much smaller than the protoplanetary mass. As the protoplanet becomes more massive because of further accretion of planetesimals, it gathers the nebular gas more and more to form a dense atmosphere. In such a stage, the accretion of planetesimals plays a primary role in the structure of the atmosphere in two different manners. An increase in the protoplanetary mass caused by the accretion of planetesimals leads to an increase in gravity force, thereby making the atmosphere compact. On the other hand, a large amount of the gravitational energy is released at the bottom of the atmosphere by incoming planetesimals, so that

the protoplanetary atmosphere is warmed and lifted up against the gravity force. By the balance between these opposite effects, the atmosphere can be completely in hydrostatic equilibrium.

When the protoplanet grows beyond a certain level of mass, the mass of the atmosphere occupies a substantial portion of the protoplanetary mass and acts as a source of the gravity force. That is, the protoplanetary atmosphere comes to the so-called self-gravitating system, which is essentially different from the usual physical system in the sense that it has a negative heat capacity as a whole (such a self-gravitating atmosphere and the central solid part are called the *envelope* and the *core*, respectively). Radiative loss from the surface of the envelope (i.e., the luminosity) inevitably leads to an increase in the internal energy of the envelope. On the other hand, the gravitational energy of the envelope must decrease because of the energy conservation. In other words, the envelope contracts gravitationally, more or less, because of the radiative loss, so that it is never maintained in hydrostatic equilibrium.

In the case of the protoplanet embedded in the nebula, the system is not closed but open, because fresh nebular gas can enter the system when the envelope contracts (e.g., Miki 1982). The contraction of the envelope leads not only to release of its own gravitational energy, but also to enhancement of its self-gravity. When the mass of the core reaches a certain critical mass (which is called *the critical core mass*), the latter effect dominates the former one, resulting in acceleration of the gas accretion. In this way, the protoplanet captures the surrounding nebular gas and becomes a massive gaseous planet.

As understood from the above-mentioned formation process, the conditions for a protoplanet to become a Jupiter-like planet are (1) that the mass

of the protoplanet (i.e., the solid core) reaches the critical core mass and (2) that the protoplanet captures a significant amount of the nebular gas within a suitable time. Apparently, the inner planets of the solar system did not satisfy these two conditions, but those of the extrasolar systems did. How large cores can be formed will be constrained by the isolation mass (see §1.2.1 for the definition), which is given by the planetary accretion theory. Furthermore, as far as the giant planets of the solar system are concerned, the current masses of the central cores, which are provided by the studies of the internal structures of Jupiter, Saturn, Uranus, and Neptune, offer additional constraints (see §1.2.2). On the other hand, "the suitable time" included in Condition (2) will be suggested by the observationally inferred lifetime of the nebula (see §1.2.3). Our main purpose is to show that protoplanets with the masses given by the studies of planetary accretion and the internal structures can capture sufficient amounts of the nebular gas within the lifetime of the nebula.

1.2 Theoretical and Observational Constraints

1.2.1 Theory of Planetary Accretion

Accretion rate of a protoplanet (i.e., a solid core) is quite important to the formation theory of the giant planets. It gives not only formation time of a solid core, but also energy input rate to the envelope. Hence, we should know it in detail. As a result of the recent progresses in the theory of planetary accretion, the accretion process of protoplanets has been clarified to a great extent.

Supposing that a protoplanet is surrounded by an assembly of planetesi-

mals, we can write growth rate of the protoplanet, $\dot{M}_{\rm c}$, as (Safronov 1969),

$$\dot{M}_{\rm c} = \rho_{\rm d} \pi R_{\rm c}^2 \Theta_{\rm g} v_{\rm r} \simeq \Sigma_{\rm d} \pi R_{\rm c}^2 \Theta_{\rm g} \Omega_{\rm K}, \tag{1}$$

where $\rho_{\rm d}$ and $\Sigma_{\rm d}$ are, respectively, the spatial density and surface density of the assembly of planetesimals, $R_{\rm c}$ the radius of the protoplanet, $v_{\rm r}$ the velocity dispersion (i.e., the sum of random velocities of the protoplanet and the planetesimals), and $\Omega_{\rm K}$ the Keplerian frequency. In Eq. (1), we used the relation $\rho_{\rm d} \simeq \Sigma_{\rm d} \Omega_{\rm K}/v_{\rm r}$ where $\Omega_{\rm K}/v_{\rm r}$ represents the thickness of the planetesimal disk (e.g., Hayashi *et al.* 1985). Furthermore, $\Theta_{\rm g}$ (which is often called the Safronov number) is a factor representing the gravitational focusing effect and given by (Safronov 1969)

$$\Theta_{\rm g} = 1 + \frac{v_{\rm esc}^2}{v_{\rm r}^2}, \tag{2}$$

where $v_{\rm esc}$ is the escape velocity from the protoplanet ($= \sqrt{2GM_{\rm c}/R_{\rm c}}$). The larger $\Theta_{\rm g}$ yields the higher $\dot{M}_{\rm c}$.

In the early stage of planetary accretion, the random velocity of a protoplanet is suppressed to be lower than that of planetesimals because of a dynamical friction between the protoplanet and the planetesimals, so that $v_{\rm r}$ is almost equal to the random velocity of the planetesimals. Especially in the stage where the mass of the protoplanet is small, the random velocity of the planetesimals is determined so that a stirring effect between the planetesimals balances with a dissipative effect of gas drag and is maintained to be very low. In this case, since $v_{\rm r}$ does not depend on the mass of the protoplanet, the relation between the growth rate and mass of the protoplanet is given by

$$\frac{M_{\rm c}}{\dot{M}_{\rm c}} \propto \frac{M_{\rm c}}{R_{\rm c}^2 v_{\rm esc}^2} \propto M_{\rm c}^{-1/3}. \tag{3}$$

This equation means that a large protoplanet grows more rapidly than smaller planetesimals. Such a stage is called the runaway growth stage (Greenberg *et al.* 1978; Wetherill and Stewart 1989) and the growth rate of the protoplanet is quite high because of small $v_{\rm r}$ (i.e., large $\Theta_{\rm g}$).

However, the initial runaway growth of the protoplanet is soon followed by slow growth (Ida and Makino 1993) when the protoplanet becomes large enough to enhance the random velocity of neighbor planetesimals almost to $v_{\rm esc}$. The protoplanet spends most of its growth period in this stage rather than in the runaway growth stage. In such a stage, the random velocity of the planetesimals is determined by the balance between the stirring effect caused by the protoplanet and the dissipative effect of the gas drag. As a result, the growth time, $\tau_{\rm c}$, required for a protoplanet located at the semimajor axis, a, to grow to the mass, $M_{\rm c}$, can be estimated as (Tanaka and Ida 1999)

$$\tau_{\rm c} = 5.8 \times 10^7 \left(\frac{M_{\rm c}}{10 M_\oplus}\right)^{1/3} \left(\frac{\Sigma_{\rm d}}{\Sigma_{\rm d}^{\rm H}}\right)^{-1} \left(\frac{a}{5{\rm AU}}\right)^{31/12} \left(\frac{m}{10^{20}{\rm g}}\right)^{1/9} {\rm yr}, \qquad (4)$$

where m is typical mass of planetesimals (note that the above equation is valid only for the outer region of the solar system, i.e., $a > 2.7$AU). Here, the superscript $^{\rm H}$ means the value prescribed by the so-called minimum-mass solar nebula model (Hayashi 1981), which has been widely adopted as the standard model of the initial condition for the solar system formation.

The behavior of planetary accretion in the slow growth stage is qualitatively different from that in the runaway growth one. That is, the larger protoplanet grows *less* rapidly than the smaller one in the slow growth stage (i.e., $M_{\rm c}/\dot{M}_{\rm c} \propto M_{\rm c}^{+1/3}$), while the larger one grows *more* rapidly than the smaller one in the runaway growth stage (i.e., $M_{\rm c}/\dot{M}_{\rm c} \propto M_{\rm c}^{-1/3}$). Suppose that a protoplanet has entered the slow growth stage and the other planetesimals

stay in the runaway growth one. The largest one of the planetesimals grows faster than the others to become a protoplanet and, furthermore, faster than the protoplanet which stays in the slow growth stage. This process occurs successively to form several protoplanets. According to N-body simulations by Kokubo and Ida (1998), the several protoplanets are formed with the orbital separations of about 10 times as large as their own tidal radii; the separation is caused by orbital repulsion. In such a stage, the growth rate of the protoplanet decreases because of depletion of planetesimals, so that the growth of the protoplanets no longer proceeds. The protoplanetary mass at this stage is called the isolation mass, $M_{\rm iso}$, and given by (Kokubo and Ida 1998)

$$M_{\rm iso} = \begin{cases} 0.1 \times \left(\dfrac{\Sigma_{\rm d}}{\Sigma_{\rm d}^{\rm H}}\right)^{3/2} \left(\dfrac{a}{1{\rm AU}}\right)^{3/4} M_\oplus & \text{for } a < 2.7{\rm AU}, \\ 1.7 \times \left(\dfrac{\Sigma_{\rm d}}{\Sigma_{\rm d}^{\rm H}}\right)^{3/2} \left(\dfrac{a}{5{\rm AU}}\right)^{3/4} M_\oplus & \text{for } a > 2.7{\rm AU}. \end{cases} \tag{5}$$

As found from this equation, as far as the minimum-mass solar nebula is considered, at most $2M_\oplus$ cores can be formed in Jupiter's region. Furthermore, only about $0.01M_\oplus$ cores can be formed around the locations of the detected extrasolar planets (~ 0.1AU).

1.2.2 Current Core Masses of Our Giant Planets

The model of the giant planet formation in the solar system should be constructed based on the constraints provided by the studies of the internal structures (especially, the masses of the cores) of Jupiter, Saturn, Uranus, and Neptune. The estimation of the current core masses involves the calculations of interior models matching the observed gravitational fields. Each of the four giant planets is believed to consist of a central dense core and a surrounding

gaseous envelope composed by hydrogen, helium, and small amounts of heavy elements. Although relatively large core masses of Jupiter and Saturn ($10-30M_{\oplus}$) were estimated in the previous works (see Stevenson (1982a) for a review), the recent studies do not necessarily suggest the existence of such large cores; the estimated core masses are $0-10M_{\oplus}$ and $6-15M_{\oplus}$ for Jupiter and Saturn, respectively (see Wuchterl *et al.* (2000) for a recent review). The main reason for the discrepancy is that the determination of the core mass is very sensitive to changes in the equation of state and presumed chemical compositions. On the other hand, Uranus and Neptune have large cores with masses of $70-90$ % of their total mass. Each value of the core mass offers an upper limit on the critical core mass for each planet.

It should be noted that the estimated core mass of Jupiter is very small compared to that estimated by the previous workers. As described in §1.3, the previous theory of the giant planet formation was constructed in the belief that Jupiter had a central core with mass of $10-30M_{\oplus}$.

1.2.3 Lifetime of a Nebula

There is another constraint on the time of the giant planet formation. All the planets of the solar system must have formed in 4.6 billion years, i.e., the solar age. In addition, dissipation time of a nebula (which is often called lifetime of a nebula) places a strict constraint on the formation of the giant planets. Observations of pre-main-sequence stars based on infrared emission in excess of stellar photospheric fluxes (Strom *et al.* 1993) or emission at the frequencies of the rotational transitions of CO molecules (Zuckerman *et al.* 1995) show that many of them have optically thick disks. The former observations suggest that such disks evolve from optically thick

to optically thin structures in about 1×10^7yr. The latter ones show that the CO lines are not detected around the stars with ages of more than about 1×10^6yr. From these observations, the typical lifetime of nebulae is inferred to be $1 \times 10^6 - 1 \times 10^7$yr. If this estimation is correct, it follows that the giant planets had to form within a period of 1×10^7yr after the central star formed. However, it is a matter of controversy whether these observational results represent the complete dissipation of the nebulae. The depletion of the infrared excess indicates only that of dust particles. In addition, the depletion of CO molecules may represent CO freeze-out onto cold dust particles. Furthermore, the dissipation processes are theoretically unclear. At present, it will be sensible to consider that the lifetime of a nebula is *of the order of* 10^7yr (see Thi *et al.* 2001).

1.2.4 Masses of Nebulae

To explain the formation of a variety of planetary systems, we should take a variety of planet-forming nebulae, in particular, nebular masses, into account. The observations of nebulae around young stars show that the nebular masses range from $0.005M_\odot$ to $0.2M_\odot$ (e.g., Beckwith and Sargent 1996). On the other hand, the minimum-mass solar nebula model, which we usually use, were constructed under the assumption that the planets of the solar system were formed near their present locations through the collection of all the local solid materials (Hayashi 1981). The mass of the minimum-mass solar nebula is about $0.01M_\odot$[1]. Thus, we can consider the formation of planetary systems in the nebulae whose masses are about 10 times as large

[1]Exactly speaking, the total mass of solid materials is inferred to be about $1 \times 10^{-4}M_\odot$ in the minimum-mass solar nebula model. On the other hand, the mass of gas is estimated under the assumption that it is about 100 times as large as that of solid materials.

as that of the minimum-mass solar nebula. Furthermore, even in the case of the solar system, we can consider somewhat a larger amount of materials compared with that of the minimum-mass solar nebula, because not all the solid materials are considered to have been taken in the planets.

When we consider dense nebulae, we have to keep in mind whether the nebulae are stable against the gravitational instability of a gaseous disk or not. If the nebular density is so high that the disk instability occurs, a giant planet should be formed through the disk instability rather than the nucleated instability, because the formation time through the disk instability is much shorter than that through the nucleated instability. The condition for the gravitational instability of a Keplerian rotating disk is given by Toomre (1964) as

$$\Sigma_0 \gtrsim \frac{c_S \Omega_{\rm K}}{\pi G}, \tag{6}$$

where Σ_0 is the surface density of the nebular gas and c_S is the sound velocity of the nebular gas. Writing the above equation in terms of the density, ρ_0, we obtain

$$\begin{aligned} \rho_0 > \rho_{0,\rm cr}^{\rm disk} &\simeq 9.3 \times 10^{-8} \left(\frac{a}{1\rm AU} \right)^{-3} \rm gcm^{-3} \\ &\simeq 78 \left(\frac{a}{1\rm AU} \right)^{-1/4} \rho_0^{\rm H}, \end{aligned} \tag{7}$$

where $\rho_{0,\rm cr}^{\rm disk}$ is the critical density for the disk instability and $\rho_0^{\rm H}$ is the density given by the minimum-mass solar nebula model (see Eq. (29)).

1.3 Review of Previous Works on the Giant Planet Formation

1.3.1 Pioneering Works

The basic concept of the nucleated instability model is as follows. A relatively massive solid core grown through planetesimal accretion attracts the surrounding nebular gas gravitationally to form a gaseous envelope. The envelope is defined as a gas inside a sphere with the surface where the gravity due to the solid core (plus the envelope) balances either with the tidal force caused by the central star or with a repulsive force originating from thermal motion of the nebular gas; outside the sphere, the gas cannot be gravitationally bounded because of the Keplerian shear motion or thermal one. The radius of the sphere is called the planetary radius, at which the envelope fits smoothly onto the nebula. As the core grows, the planetary radius expands and, furthermore, the envelope contracts. As a result, there occurs further gas accretion leading to an increase in the mass of the envelope.

This concept is based on the pioneering work done by Perri and Cameron (1974). They constructed models of the gaseous envelope assuming that the envelope was in hydrostatic and thermal equilibrium and was wholly convective. By integrating the equation of hydrostatic equilibrium inwards from the planetary radius, which was determined by the planetary mass, to a radius at which the mean density predicted by the envelope solution was equal to the presumed core density, they determined the relation between the core mass and the planetary total mass. They found that there existed a critical core mass, beyond which no hydrostatic solution could be obtained, and predicted that the envelope collapsed onto the core to be tightly bounded

when the core mass exceeded the critical core mass. However, the obtained values of the critical core mass were very large ($60 - 120 M_\oplus$) compared to those which had been inferred by the studies of the internal structures of the four giant planets ($10 - 30 M_\oplus$; see Stevenson 1982a). They also pointed out that appropriate treatment of the thermal structure of the envelope was required for explanation of the present core mass, because the value of the critical core mass was very sensitive to an adopted adiabat and the radiative transfer became important, at least, in the outer parts of the envelope.

This problem was challenged by Mizuno (1980) following Mizuno *et al.* (1978). He took radiative transfer as well as convective one into account according to the familiar way for determining stellar structures. Calculations of radiative transfer require an exact knowledge of the amount of energy flux in the envelope as well as opacity. Mizuno (1980) considered that the energy was supplied at the surface of the core by planetesimals that fell onto the core at a constant rate of $1 \times 10^{-6} M_\oplus$/yr. On the other hand, he considered gas and grains as the opacity sources. The grain opacity depends on the abundance and sizes of grains, both of which are quite uncertain. Therefore, he treated the grain opacity as a parameter. Following Perri and Cameron (1974)'s procedure, he obtained the critical core mass that was smaller ($\sim 10 M_\oplus$) than that by Perri and Cameron (1974). In addition, they found numerically and explained analytically that the value of the critical core mass scarcely depended on the distance of a planet from the Sun (also see Stevenson 1982b). However, there remained an important problem, because the planetary total mass (almost twice as large as the core mass) at the critical point was much smaller than the current Jupiter's mass and Saturn's mass. This indicated

the need for evolutionary calculations beyond the critical core mass.

Bodenheimer and Pollack (1986) first performed the quasi-static evolutionary calculations of the envelope in the similar way to that of evolutionary simulations of pre-main-sequence and post-main-sequence stars except the existence and growth of a central incompressible core. That is, they assumed that the envelope was in hydrostatic equilibrium but not in thermal one. For the parameters almost the same as those used by Mizuno (1980), they showed that, beyond the critical core mass obtained by Mizuno (1980), the envelope increased in mass much more rapidly (but never collapsed) than the core to the present mass in a negligibly short period compared to that needed for the arrival at the critical core mass.

The main conclusions of these pioneering works were (1) that the critical core mass was about $10M_{\oplus}$, (2) that the accretion time of the envelope was much shorter than that of the core, and (3) that the critical core mass and the accretion time of the envelope scarcely depend on the distance from the Sun. These conclusions were widely accepted, because both the value of the critical core mass itself and the similarity of it among the four giant planets were consistent with the fact deduced in 1980s by the studies of the internal structure of the four giant planets that all the four giant planets had cores with masses of about $10M_{\oplus}$. However, the value of the critical core mass (Conclusion (1)) is not consistent with the isolation mass (see §1.2.1) and the present core mass of Jupiter (see §1.2.2). Furthermore, the formation of a $10M_{\oplus}$ core, for example, at 0.05 AU, requires the initial surface density of solid materials more than 100 times as high as that of the minimum-mass solar nebula. Such a dense nebula has not been detected yet (see §1.2.4).

Finally, it may have to be noted that Wuchterl (1991) performed dynamically (i.e., without assuming hydrostatic and thermal equilibrium) evolutionary calculations of the envelope. He obtained a surprising result that a hydrodynamical instability occurred and a substantial fraction of the envelope mass was ejected on a dynamical timescale just after the mass of the core exceeded the critical core mass. This instability probably stems from the so-called κ-mechanism (see Kippenhahn and Weigert 1990) in which amplitudes of oscillation grow because of injection of energy by enhanced absorption of radiation at maximum compression and enhanced emission at maximum expansion. The occurrence of this instability is, as a matter of course, very sensitive to opacity data, in particular, the grain opacity near evaporation points of grains (Wuchterl 1995). It is difficult to know the grain opacity exactly, mainly because it requires an exact knowledge of compositions of grains (cf. Pollack *et al.* 1985). So, whether such instability really happens or not is controversial. Actually, Tajima and Nakagawa (1997) carried out a careful check on the dynamical stability of the envelope during its evolution using quasi-static calculations, but they could not detect the occurrence of such instability. Therefore, we will not consider the dynamical instability in this study.

1.3.2 Recent Progresses

As described in §1.2.1, the growth rate of a solid core (i.e., the core accretion rate) changes considerably from stage to stage, namely from the runaway growth stage to the isolation one followed by the slow growth one. Nevertheless, the pioneering works (Mizuno 1980; Bodenheimer and Pollack 1986) assumed constant core accretion rates. This point was improved by

Pollack *et al.* (1996), who simulated the gas accumulation process combined with a time-dependent core accretion rate based on the numerical calculations by Greenzweig and Lissauer (1992). They concluded that, if the initial surface density of solid materials was 3 - 4 times as high as that of the minimum-mass solar nebula, cores with masses of more than $10M_{\oplus}$ could form to capture the nebular gas comparable in mass to the present envelope within a period of $(1-10)\times10^6$yr. However, the core accretion rate used by them was debatable. Especially, the Safronov number, $\Theta_{\rm g}$, was quite large ($\Theta_{\rm g} \simeq 1\times10^4 - 1\times10^5$) because they neglected the stirring effect caused by protoplanets, so that the cores with masses of more than $10M_{\oplus}$ could form in $(1-10)\times10^5$yr. As pointed out by Bryden *et al.* (2000), such a large $\Theta_{\rm g}$ cannot be realized unless any special situations are set up. Although the situation was not realistic one, it is worth while noting that they found a new dominant phase (called "Phase 2") after the isolation, during which both accretion rates of solids and gas were relatively small and almost constant with time. Such a phase seems to be consistent with the prediction of the recent theory of planetary accretion (Kokubo and Ida 1998). This phase is very important, because it would occupy most of the formation period. However, the mechanism involved in this phase was not clarified.

All of the above-mentioned previous works focused on the giant planets of the solar system. Recently, Papaloizou and Terquem (1999) and Bodenheimer *et al.* (2000) constructed models of the formation of the extrasolar planets orbiting close to the central stars. The issue is particularly challenging, since it is difficult for a core with mass of about $10M_{\oplus}$ to form in such an inner region, as implied in Eq. (5). To overcome this difficulty, Pa-

paloizou and Terquem (1999) proposed that a protoplanetary core grew in mass owing to significant core accretion through its inward migration (Lin and Papaloizou 1993; Ward 1997) and then reached the massive critical core mass ($20-40M_{\oplus}$) after its journey from 5AU to $\sim$ 0.1AU. However, whether the migration of protoplanets actually occurred or not is still an unsolved problem. The giant planets, including our four ones, orbit at a variety of semimajor axes ranging from 0.05 AU to 30.1 AU. There is no answer to how they could stop in their current positions if all of the planets formed through orbital migration.

In contrast, Bodenheimer *et al.* (2000) investigated the possibility of the *in situ* formation. They assumed a high core accretion rate of $1 \times 10^{-5} M_{\oplus}$/yr produced by plenty of solid materials with surface density of about 40 times as high as that of the minimum-mass solar nebula or maintained by delivery of planetesimals from the outer region to the formation site. They also showed that a protoplanetary core could grow to $30-50M_{\oplus}$ and then could capture a large amount of gas in situ. However, the existence of such a dense nebula has not been observationally ensured (see §1.2.4). In addition, the mechanism for the delivery of planetesimals such that the high core accretion rate can be maintained is quite unclear. Whether such an *ad hoc* assumption is really needed or not should be investigated.

1.4 The Purpose of This Study

The previous workers (Pollack *et al.* 1996; Papaloizou and Terquem 1999; Bodenheimer *et al.* 2000) constructed formation models for some of the detected giant planets (including our giant planets). They had to set

some special situations in which massive cores ($> 10M_{\oplus}$) could form in short periods, because they believed that smaller cores were insufficient to capture a large amount of nebular gas. The recent planetary accretion theory, however, does not suggest that cores can grow in mass to about $10M_{\oplus}$ (see §1.2.1). The recent study of the internal structure of Jupiter also denies the existence of such a large core (see §1.2.2). Furthermore, the situations they considered were not necessarily realistic ones, as pointed out in the previous section.

In this study, we will investigate the formation of the giant planets in the manner apparently different from that of the previous works. We do not consider a particular planet for a while, but dedicate ourselves to know the dependences of the accretion time of the envelope as well as the critical core mass on the parameters included in the nucleated instability model. We can never conclude the need for the special settings introduced by the previous workers, until we obtain a precise knowledge of the dependences. As a result of our extensive investigation, we will show that Jupiter can be formed within the standard context of planetary formation and, furthermore, the small mass of the core which triggers considerable gas accretion is consistent with that estimated by the study of the internal structure of Jupiter. We will also show that the extrasolar planets orbiting close to the central stars can form at their present locations in a reasonable situation. Although the in situ formation of Saturn, Uranus, and Neptune is found to be difficult, we can propose a formation scenario (i.e., outward migration of protoplanets) based on our obtained information and understanding.

As readily conjectured from the formation processes described in §1.1, the onset time of the considerable gas accretion depends on the core accre-

tion rate, which determines the amount of the energy input to the envelope. The accretion rate changes from stage to stage and ranges widely depending on distance from the central star. The isolation of protoplanets from planetesimals would really happen. In that case, the accretion rate would almost vanish. Furthermore, the opacity is also an important quantity, since it governs the thermal response of the envelope. As mentioned in §1.3.1, the opacity sources are gas and grains in our problem. In particular, the grain opacity is poorly understood because we have no precise knowledge of both the abundance and sizes of grains in the ancient envelope.

We should take into account a wide range of the nebular density and temperature as well as the position of a protoplanet to explain the formation of the extrasolar planets. These quantities are the outer boundary conditions for the envelope. Although the weak dependence of the outer boundary conditions were shown by several workers (Mizuno 1980; Stevenson 1982b; Bodenheimer and Pollack 1986), the conclusion does not hold true in general. As pointed out by Wuchterl (1993), the critical core mass depends on the outer boundary conditions in the nebula with high density such that the outer envelope becomes convective (see §4.2.1). Note that Wuchterl (1993) investigated the dependence of the critical core mass on the nebular density only at 5.2 AU and found that the critical core mass rapidly decreases with the increasing density for very large densities. However, the densities he considered were unrealistically high (i.e., much larger than the critical density for the disk instability).

In §2, we describe the assumptions, the basic equations, and the parameters (i.e., the core accretion rate, the grain opacity and the outer bound-

ary conditions). In §3, we present our numerical methods to simulate the accretion and evolution of a protoplanetary envelope. In §4.1, we see the dependences of the accretion time of the envelope and the critical core mass on the core accretion rate and the grain opacity. Furthermore, we investigate the case in which the core accretion rate stops abruptly. In §4.2, we show the dependence of the critical core mass on the density and temperature of nebular gas and the distance from the central star. In §5, applying our numerical results, we discuss the formation of the various giant planets, i.e., the extrasolar giant planets as well as our giant planets.

2 Theoretical Model of a Protoplanet

2.1 Assumptions

We consider a double-layered protoplanet (i.e., a protoplanet composed of a solid core and a gaseous envelope), which is embedded in the nebula. We make the following assumptions, which are similar to those used by Mizuno (1980) and Bodenheimer and Pollack (1986).

1. The protoplanet has a spherically symmetric structure.

2. The envelope is always in hydrostatic equilibrium.

3. The core is inert and has a constant density, ρ_c, of $5.5 \mathrm{g/cm^3}$.

4. The envelope has a uniform chemical composition with the solar system abundances: the mass fractions of hydrogen, helium, and heavy elements are 0.740, 0.243, and 0.017, respectively.

5. The energy source of the envelope is the kinetic energy of planetesimals falling onto the core at a rate, $\dot{M}_c$ (see §2.4). All of their kinetic energy is dissipated only at the bottom of the envelope. The energies due to radioactive decay and the cooling of the core are not considered.

6. The envelope connects smoothly with the nebula at the presumed planetary radius (see Eq. (9)). The nebular gas exists during the entire time of our simulation, namely, dissipation of the nebular gas is not considered.

7. The radiative and convective regions of the envelope are separated completely by the Schwartzschild criterion (see Eq. (20)).

We make some comments on the above assumptions. Assumption 1 is made apparently for simplicity. There will be additional forces, which distort the envelope from the spherical geometry, such as a tidal force caused by the central star and the centrifugal force due to rotation of the protoplanet. The former force influences only a narrow region near to the surface of the envelope, so its effect is a trivial one for the gravitational stability of the envelope (Mizuno *et al.* 1978). The latter force may be more important than the former one, because it can affect a deep part of the envelope. The envelope can be considered to have angular momentum more or less, since it captures the gas orbiting around the central star. Unfortunately, it is highly uncertain how much angular momentum is carried into the envelope and how efficiently it is removed from the envelope. We neglect the effect in this study. This will be our future work.

Assumption 2 can be readily justified because the characteristic time of the gravitational contraction of the envelope (which is equal to the thermal relaxation time) is of the order of 1×10^5 yr or more, whereas that of the hydrodynamic change is several hours. By Assumption 3, we are not concerned with the detailed structure of the core in finding the hydrostatic structure of the protoplanet. Exactly speaking, the mean density of the core increases slightly as the core mass (as well as the core radius) increases with time because of planetesimal accretion. This is not so important because it is already known that this effect changes the critical core mass only by a few percents (Mizuno *et al.* 1978).

One may also be anxious for the justification of the second part of Assumption 5. Certainly, planetesimals falling through the envelope would suf-

fer from fragmentation due to dynamical pressure and evaporation because of the hot environment, so a part of their kinetic energy must deposit in the envelope. However, it has already been known that, even if we take into account these processes of the energy deposition, the critical core mass and the accretion time of the envelope are changed only by at most 10% (Miyoshi *et al.* 1996; Pollack *et al.* 1996). It should be noted here that our mathematical formalism includes automatically the energy liberation due to the gravitational contraction of the envelope and the work done by the growing core (see §2.2).

Finally, candidates for the planetary radius where the envelope connects smoothly with the nebula (Assumption 6) are the Hill radius, $R_{\rm H}$, and the Bondi radius, $R_{\rm B}$:

$$R_{\rm H} \equiv \left(\frac{M_{\rm t}}{3M_\odot}\right)^{1/3} a \quad \text{and} \quad R_{\rm B} \equiv \frac{GM_{\rm t}}{c_S^2}, \tag{8}$$

where $M_{\rm t}$ and $M_\odot$ are, respectively, the masses of the protoplanet and the Sun and c_S is the sound velocity of the nebular gas. At $r > R_{\rm H}$, the tidal distortion is so effective that the gas cannot be gravitationally bounded by the planet. On the other hand, at $r > R_{\rm B}$, a repulsive force originating in the thermal motion of gas dominates the gravity force of the planet. Hence, we should define the planetary radius, R, by the smaller of the two:

$$R = \min[R_{\rm H}, R_{\rm B}]. \tag{9}$$

The Hill radius and the Bondi radius depend on $M_{\rm t}$ in the different ways, so that $R_{\rm B}$ exceeds $R_{\rm H}$ at a certain $M_{\rm t}$. The total mass when $R_{\rm B} = R_{\rm H}$ is given by

$$M_{\rm t} = \sqrt{\frac{G}{3}\left(\frac{c_S^2}{G}\right)^3 \frac{1}{\Omega_{\rm K}^2}}$$

$$= 12.3 M_\oplus \left(\frac{T_0}{T_0^{\rm H}}\right)^{3/2} \left(\frac{a}{1{\rm AU}}\right)^{3/4}, \tag{10}$$

where T_0 and $T_0^{\rm H}$ are the temperatures of the nebula and of the minimum-mass solar nebula (see Eq. (30); Hayashi 1981), respectively, and we used the relation, $GM_\odot = \Omega_{\rm K}^2 a^3$.

2.2 Basic Equations

We use a set of the equations that is similar to that for the calculations of the quasi-static stellar evolution. In simulating the quasi-static stellar evolution, we pursue time-variation of various quantities of a mass element. It, therefore, simplifies matters that we use the Lagrangian coordinate as an independent variable, which moves with bulk motion of a mass shell. We define the Lagrangian coordinate, M_r, by the mass contained within a sphere with radius r:

$$M_r \equiv \int_0^r 4\pi r'^2 \rho dr', \tag{11}$$

where ρ is the density. In simulating the quasi-static evolution of the protoplanetary envelope, however, situation is somewhat different because the core mass increases with time, t, because of planetesimal accretion. That is, M_r is also a function of t and not purely the Lagrangian coordinate. We do not know a priori how the radius r of a mass shell changes, but know how M_r increases with time, i.e.,

$$\frac{dM_r}{dt} = \dot{M}_{\rm c} \Theta(r - r_{\rm c}), \tag{12}$$

where $r_{\rm c}$ is the core radius and $\Theta(x)$ is the step function of a variable x. Thus, we also choose $(M_r,\, t)$ rather than $(r,\, t)$ as a set of independent variables.

Since we have assumed that the protoplanetary envelope is in hydrostatic equilibrium, we can write the equation describing the mechanical structure of the envelope as

$$\frac{\partial P}{\partial M_r} = -\frac{GM_r}{4\pi r^4}, \tag{13}$$

where P is the pressure and $\partial/\partial M_r$ is the partial derivative at constant t. By the definition of M_r (see Eq. (11)), the equation for $r(M_r)$ is given by

$$\frac{\partial r}{\partial M_r} = \frac{1}{4\pi r^2 \rho}. \tag{14}$$

For Eqs. (13) and (14), we need a relation between P and ρ, which is given by the equation of state. The envelope gas, in particular, near the surface of the core is highly condensed, so the assumption of an ideal gas is not valid. In this study, we use the equation of state for a nonideal gas given by Saumon *et al.* (1995) interpolated to our presumed composition[2]. The equation of state is written symbolically as

$$\rho = \rho(P, T), \tag{15}$$

where T is the temperature. As seen from Eq. (15), we have to know the temperature as a function of M_r.

The temperature distribution is determined by energy transfer in the envelope. In this study, we consider two kinds of transport mechanisms. One of them is radiative transfer. Since the protoplanet of interest is embedded in the relatively dense background gas, the optical depth measured from the planetary radius is much greater than unity. In this case, the temperature

[2]Ikoma *et al.* (1998) and Ikoma *et al.* (2000) performed the calculations that are the same as those done in §4.1. They used the ideal equation of state. Their results about the critical core mass and the accretion time of the envelope are changed by at most 10% if nonideal one is used.

distribution is well described by the radiation-conduction (in other words, diffusion) approximation. The basic concept is as follows. Each mass shell with radius r is a blackbody and emits photons with energy flux of $4\pi r^2 \sigma_{\rm SB} T^4$ ($\sigma_{\rm SB}$: the Stefan-Boltzmann constant). The emitted photons travel over their mean free paths ($\simeq 1/\bar{\kappa}\rho$, where $\bar{\kappa}$ is the cross section per unit mass) freely and deposit their energy at the point where the photons collide with the gas. According this concept, the temperature distribution is derived as (see, for example, Shu (1991) for the derivation)

$$\frac{\partial T}{\partial M_r} = -\frac{GM_r}{4\pi r^4}\frac{T}{P}\nabla_{\rm rad}, \tag{16}$$

where

$$\nabla_{\rm rad} \equiv \frac{d\ln T}{d\ln P} = \frac{3}{64\pi\sigma_{\rm SB}G}\frac{\kappa L_r P}{M_r T^4} \tag{17}$$

and κ is the Rosseland mean opacity and L_r the energy flowing outward through a spherical surface of radius r. The sources of the opacity are gas and grains. For the gas opacity table, we use one that D. Alexander kindly calculated by our request (cf. Alexander and Ferguson 1994). On the other hand, we obtain the grain opacity from Pollack *et al.* (1985), who presumed dust grains with an interstellar size distribution and took into account magnetite, iron, water, and silicate as particulate species. Each species evaporates at each evaporation temperature and, therefore, the grain opacity decreases abruptly at several evaporation points (see §2.4 for the detail description).

Another transport mechanism is convection, which is characterized by upward and downward macroscopic fluid motions. If a fluid element decreases (or increases) its temperature during the upward (or downward) motion more slowly than the environment, the temperature of the element is hotter (or

cooler) than that of the environment. In this case, the element will exchanges its energy with the environment at its new position, resulting in the outward energy transfer. A model on the basis of this picture, *the mixing length model* (Böhm-Vitense 1958), has been widely accepted by the workers on studies of stellar evolution and we also use it. In the mixing length model, fluid elements move over a distance (which is called the mixing length) adiabatically and then exchange their energy with their surroundings. According to this model, the temperature distribution is given by

$$\frac{\partial T}{\partial M_r} = -\frac{GM_r}{4\pi r^4}\frac{T}{P}\left(\nabla_{\rm ad} + \delta\nabla_{\rm ad}\right), \tag{18}$$

where

$$\nabla_{\rm ad} = \left(\frac{\partial \ln T}{\partial \ln P}\right)_S \tag{19}$$

and $\delta\nabla_{\rm ad}$ is the deviation from $\nabla_{\rm ad}$ and is principally determined by L_r (see Kippenhahn and Weigert (1990) for the detailed description). Hereafter, we write $\nabla_{\rm ad} + \delta\nabla_{\rm ad}$ simply as $\nabla_{\rm conv}$.

The criterion, which separates a radiative region and a convective one (i.e., the Schwartzschild criterion), is easily derived. Suppose that the temperature gradient with respect to the pressure of the surroundings determined by radiation, $\nabla_{\rm rad}$, is smaller than the adiabatic gradient, $\nabla_{\rm ad}$. As a result of an infinitesimal, upward displacement of a fluid element, the temperature of the fluid element is lower than that of its surroundings, namely, the density of the fluid element is higher than that of the surroundings. In this case, the fluid element is pushed back to its original position. In the opposite case, the fluid element can move upwards more and more by the increasing buoyancy

force. Thus, convection occurs in the case where

$$\nabla_{\rm ad} < \nabla_{\rm rad}. \tag{20}$$

In summary, the equation for $T(M_r)$ is written as

$$\frac{\partial T}{\partial M_r} = -\frac{GM_r}{4\pi r^4}\frac{T}{P}\nabla, \tag{21}$$

where

$$\nabla = \begin{cases} \nabla_{\rm rad} & \text{for} \quad \nabla_{\rm rad} < \nabla_{\rm ad}, \\ \nabla_{\rm conv} & \text{for} \quad \nabla_{\rm rad} > \nabla_{\rm ad}. \end{cases} \tag{22}$$

If the envelope is in thermal equilibrium in the sense that there is no energy deposition everywhere in the envelope, the energy flux, L_r, is given only by incoming planetesimals at the bottom of the envelope and is spatially constant. In this case, a set of the above-mentioned equations is mathematically closed, if three boundary conditions are given. However, in our case, the envelope gas liberates its gravitational energy because of its contraction. From the first principle of thermodynamics, we obtain

$$\frac{\partial L_r}{\partial M_r} = \varepsilon_{\rm ac} - T\frac{dS}{dt}, \tag{23}$$

where $\varepsilon_{\rm ac}$ is the energy generation rate caused by incoming planetesimals. From Assumption 5, $\varepsilon_{\rm ac}$ is given by

$$\varepsilon_{\rm ac} = \frac{\delta(r - r_{\rm c})}{4\pi r^2 \rho}\int_{r_{\rm c}}^{R}\frac{GM_{r'}}{r'^2}dr'. \tag{24}$$

where δ is Dirac's delta function.

Finally, the equation for the time-variation of the protoplanetary mass, $M_{\rm t}$, can be obtained simply from Eqs. (11) and (12) (see Ikoma (1998) for the derivation):

$$\frac{dM_{\rm t}}{dt} = 4\pi R^2 \rho_0 \left(\frac{dR}{dt} - V\right) + \dot{M}_{\rm c}, \tag{25}$$

where ρ_0 and V are the density of the nebular gas and the fluid velocity at the planetary radius R, respectively. The mass of the protoplanet increases primarily because of planetesimal accretion, which is denoted by the last term of the above equation. An increase in the core mass leads to an increase in the gravity force, so that the planetary envelope contracts and, on the other hand, the planetary radius becomes large. The surrounding nebular gas flows inward to occupy the evacuated volume. This effect is expressed by the first term of the right hand side of Eq. (25).

2.3 Boundary Conditions

In the previous subsection, we obtained four differential equations, namely, Eqs. (13), (14), (21), and (23). Hence, we need four boundary conditions. Two of the four are assigned at the inner boundary (i.e., at $M_r = M_c$) and given by

$$r = \left(\frac{3M_c}{4\pi\rho_c}\right)^{1/3} \quad \text{and} \quad L_r = 0 \qquad \text{at } M_r = M_c. \tag{26}$$

Note that the energy supplied by planetesimals is included in Eq. (23). On the other hand, the two outer boundary conditions are readily given by Assumption 6;

$$\rho = \rho_0 \quad \text{and} \quad T = T_0 \qquad \text{at } M_r = M_t. \tag{27}$$

We give the nebular density, ρ_0, on the basis of that of the minimum-mass solar nebula, that is,

$$\rho_0 = c_\rho \cdot \rho_0^{\mathrm{H}}, \tag{28}$$

where ρ_0^{H} is given by (Hayashi 1981)

$$\rho_0^{\mathrm{H}} = 1.2 \times 10^{-9} \left(\frac{a}{1\mathrm{AU}}\right)^{-11/4} \mathrm{gcm}^{-3}. \tag{29}$$

In §4.1, the numerical parameter, c_ρ, is always unity, since the results obtained there scarcely depend on c_ρ. In §4.2, we consider a wide range of c_ρ, that is, from 0.1 to 100.

On the other hand, we consider two types of temperature distributions, those given by the minimum-mass solar nebula model (Hayashi 1981) and Sasselov and Lecar (2000), in §4.2. In the subsection, we are interested in the dependence of the critical core mass on the nebular temperature. In §4.1, we consider only the former, because the obtained results there also scarcely depend on T_0. In the minimum-mass solar nebula, most of the dust grains have settled down to the mid-plane of the nebula (i.e., the site of planetary formation), so the dust grains at the mid-plane can receive the energy directly from the central star and emit it to warm up the surrounding gas. In the minimum-mass solar nebula, the temperature distribution is written in the form of

$$T_0^{\rm H} = 280 \left(\frac{a}{1{\rm AU}} \right)^{-1/2} {\rm K}. \tag{30}$$

In contrast, a number of dust grains are distributed throughout the nebula in Sasselov and Lecar (2000)'s model. In this case, a blackbody-surface of the nebula (which is far from the mid-plane) receives the solar radiation and the energy is transferred toward the mid-plane of the nebula. The temperature distribution, $T_0^{\rm SL}$, is given by (Sasselov and Lecar 2000)

$$T_0^{\rm SL} = 140 \left(\frac{a}{1{\rm AU}} \right)^{-3/7} {\rm K}. \tag{31}$$

Note that $T_0^{\rm SL} < T_0^{\rm H}$ in the region of interest (i.e., $a < 100$AU). We cannot judge which nebula is appropriate for the planet-forming nebula, until

we know the abundance of the floating dust grains strongly related to the dynamical state of the nebula, which is highly uncertain.

2.4 Core Accretion Rate and Grain Opacity

As described in §1.2.1, the core accretion rate changes considerably from stage to stage. Despite such variation, we use the following simple core accretion rate taking isolation of a solid core into account:

$$\dot{M}_{\rm c}(t) = \dot{M}_{\rm c}^0 \min\left(e^{-\frac{t-t_0}{\tau_{\rm d}}}, 1\right), \tag{32}$$

where $\dot{M}_{\rm c}^0 = \dot{M}_{\rm c}(t=0)$. Until $t = t_0$, the core grows at a constant rate $\dot{M}_{\rm c}^0$; after $t = t_0$, the accretion rate decays exponentially with a typical decay time of $\tau_{\rm d}$. As shown in §4.1, we can obtain most of the information of interest even if we use such a simple core accretion rate. In this study, we restrict ourselves to two extreme cases in which $\tau_{\rm d} \to \infty$ and $\tau_{\rm d} \to 0$. The former corresponds to the case in which the accretion rate is constant (i.e., $\dot{M}_{\rm c}^0$) throughout evolution of the envelope and the latter to the case in which the accretion is halted abruptly at $t = t_0$.

As shown in the previous studies (Mizuno 1980; Stevenson 1982b), the grain opacity also plays an important role in our problem. Unfortunately, we have no knowledge about the amount and size distribution of dust grains floating in the ancient envelope. The amount of the grains in the envelope could be much smaller than that in the interstellar cloud, because almost all of the dust grains had already been in planetesimals and protoplanets. However, small grains can be replenished through evaporation and fragmentation of incoming planetesimals. The amount (and also the sizes) of the replenished grains would depend on the internal structure and dynamics of the

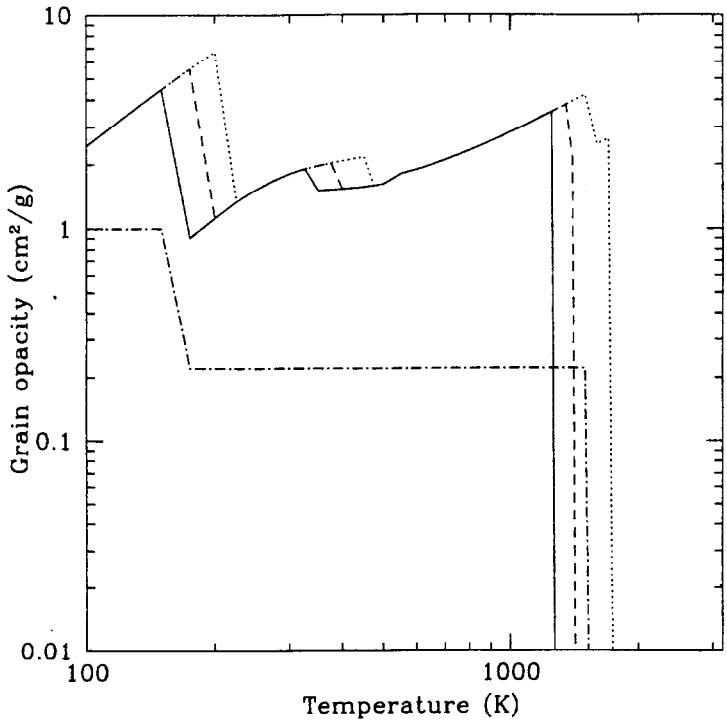

Figure 1: Grain opacity as a function of temperature. The solid, dashed, and dotted lines are the grain opacity given by Pollack *et al.* (1985) for densities of 1×10^{-10}g/cm^3, 1×10^{-8}g/cm^3, and 1×10^{-6}g/cm^3, respectively. The dot-dashed line is that given by Mizuno (1980).

incoming planetesimals in a complicated manner. Therefore, we regard the grain opacity, $\kappa_{\rm gr}$, as a parameter in the form of *the grain depletion factor*, f, which is defined by

$$f = \frac{\kappa_{\rm gr}(\rho, T)}{\kappa_{\rm gr}^{\rm P}(\rho, T)}, \tag{33}$$

where $\kappa_{\rm gr}^{\rm P}$ is the grain opacity given by Pollack *et al.* (1985).

It should be noted that Mizuno (1980), Ikoma *et al.* (1998), and Ikoma *et al.* (2000) used a rather simple grain opacity, $\kappa_{\rm gr}^{\rm M}$, instead of $\kappa_{\rm gr}^{\rm P}$ that was used by Bodenheimer and Pollack (1986), Pollack *et al.* (1996), and Bodenheimer

et al. (2000);

$$\kappa_{\rm gr}^{\rm M} = 0.78\Theta(170{\rm K} - T){\rm cm}^2/{\rm g} + 0.22\Theta(1600{\rm K} - T){\rm cm}^2/{\rm g}, \qquad (34)$$

where the temperatures 170K and 1600K correspond approximately to the evaporation temperatures of ice and rock, respectively. Figure 1 shows $\kappa_{\rm gr}^{\rm P}$ and $\kappa_{\rm gr}^{\rm M}$ as functions of temperature. From this figure, we can find that $\kappa_{\rm gr}^{\rm P}$ is larger by a factor of 10 to 20 than $\kappa_{\rm gr}^{\rm M}$ for temperatures from 200 to $\sim$ 1000K. Furthermore, while $\kappa_{\rm gr}^{\rm M}$ does not depend on the density, $\kappa_{\rm gr}^{\rm P}$ does mainly because evaporation temperatures become high with increasing density. We cannot compare the results of the above-mentioned previous works in a simple way, because of such considerable and complicated differences in the adopted grain opacity. We have to perform the calculations similar to those done by Mizuno (1980), Ikoma *et al.* (1998), and Ikoma *et al.* (2000), using $\kappa_{\rm gr}^{\rm P}$ instead of $\kappa_{\rm gr}^{\rm M}$. The grain opacity given by Pollack *et al.* (1985), $\kappa_{\rm gr}^{\rm P}$, is better than $\kappa_{\rm gr}^{\rm M}$ in the sense that $\kappa_{\rm gr}^{\rm P}$ is the Rosseland mean opacity which is required naturally by the radiation-conduction approximation. Note, however, that the compositions and sizes of grains assumed by Pollack *et al.* (1985) are not necessarily valid for those of the grains in the envelope.

3 Numerical Method

Our main interest is to know how the mass of a protoplanet increases with time. For this purpose, we perform two types of numerical calculations: static and quasi-static calculations. In the static calculation, we need one more assumption in addition to those mentioned in §2.1, i.e., the assumption that the envelope is strictly in thermal equilibrium (or , in other terms, $TdS/dt = 0$ in Eq. (23)). While the quasi-static calculation is time-consuming, the static one is accomplished in a relatively simple way. Furthermore, as shown in §4.1, the critical core mass and the luminosity at the critical core mass, which are found only with the help of the static calculations, give us a great insight into the evolutionary behavior of the envelope. In this section, we present the two methods briefly.

The numerical algorithm for the quasi-static calculation is constructed based on the so-called *relaxation method* or *Henyey method*, which was originally developed by Henyey (1957) and improved by Kippenhahn *et al.* (1967). On the other hand, the static calculations are done based on the straightforward integration method.

3.1 Essence of the Relaxation Method

For understanding our numerical method, it is helpful to show a simple example prior to the detailed description of our method. Let us consider a differential equation of the form of

$$\frac{dy}{dx} = f(x, y) \qquad \text{for} \quad x_1 \leq x \leq x_N \tag{35}$$

with the boundary condition $y(x_1) = y_1$. In order to find solution $y(x)$ numerically, we first rewrite Eq. (35) in the form of a difference equation; dividing the x-coordinate into $N-1$ zones and labeling their boundaries as $x_1, x_2, \cdots x_N$ in the positive direction of x, we obtain

$$\frac{y_{j+1} - y_j}{x_{j+1} - x_j} = \frac{f_{j+1} + f_j}{2} \left(\equiv f_{j+\frac{1}{2}}\right) \qquad \text{for} \quad j = 1, \cdots, N-1. \tag{36}$$

Introducing functions,

$$g_j(y_1, y_2, \cdots, y_N) \equiv (y_{j+1} - y_j) - f_{j+1/2}(x_{j+1} - x_j), \tag{37}$$

our present aim is to find $y_2, \cdots y_N$ which satisfy

$$g_j(y_1, y_2, \cdots, y_N) = 0 \qquad \text{for} \quad j = 1 \text{ to } N-1. \tag{38}$$

We suppose that the solution y_j is written as a sum of a guessed value y_j^0 and a correction δy_j, i.e.,

$$y_j = y_j^0 + \delta y_j \qquad \text{for} \quad j \geq 2. \tag{39}$$

Inserting Eq. (39) into Eq. (38), expanding g_j into a power series of δy_j, and ignoring terms of the second and higher orders of δy_j, we obtain a set of linearized algebraic equations,

$$g_j^0 + \sum_{k=2}^{N} \left(\frac{\partial g_j}{\partial y_k}\right)^0 \delta y_k = 0, \tag{40}$$

where superscript 0 denotes a functional value evaluated in terms of y_j^0. This linearized equation can be readily solved, for example, by the use of the matrix-inversion method. Thus, we obtain the first approximate solution to the difference equation, Eq. (38).

Replacing y_j^0 with newly found y_j and repeating the entire process mentioned above, we find the second approximate solution. By re-iterating the same procedure until all of the $|\delta y_j|$ become as small as desired, we finally obtain the solution to the difference equation with a desired accuracy. Based on the above procedure, which is called the *Newton-Raphson method* mathematically, we construct our numerical algorithm for solving the protoplanetary evolution.

3.2 Application of the Relaxation Method

3.2.1 Forms of the Equations Suitable to Our Calculation

For several numerical reasons, we should transform the basic equations presented in §2.2 to ones of the forms suitable to our numerical calculation. First, the variables, P, T, r, and L_r, vary by several orders of magnitude in the envelope. Since we have to approximate the differential equations by difference equations in order to solve them numerically, we would suffer from a considerable truncation error, if we used the linear forms of the variables. To minimize such an error, we prefer logarithmic forms to linear ones. For example, we rewrite $\partial P/\partial M_r$ as $P \cdot \partial \ln P/\partial M_r$.

Next, to the quasi-static calculation, it is most important to evaluate the time-derivative of the entropy, dS/dt, exactly. Unfortunately, we have to use tabular data of S as a function of P and T rather than analytically obtained one, because the calculation of the thermodynamic quantities is complicated and very time-consuming. Furthermore, the tabular values given by Saumon *et al.* (1995) are limited for digits, resulting in a truncation error. For this reason, we should re-express the time-derivative of S in terms of P and T

with the help of a thermodynamically identical equation, namely,

$$T\frac{dS}{dt} = C_P T\left(\frac{d\ln T}{dt} - \nabla_{\rm ad}\frac{d\ln P}{dt}\right), \tag{41}$$

where C_P is the specific heat at constant pressure. Note that, although we know other expressions for dS as a function of dP and dT, we should use this expression including $\nabla_{\rm ad}$ so that Eq. (23) becomes numerically consistent to Eq. (21) which also involves $\nabla_{\rm ad}$.

Finally, our basic equation of energy transfer, Eq. (21), includes two kinds of equations (i.e., radiative and convective transfers), the boundary of which is determined by comparison between $\nabla_{\rm rad}$ and $\nabla_{\rm ad}$. We do not know a priori where the boundary is. Hence, finding the boundary requires an iterative procedure. To avoid such a troublesome task, we combine the two equations using the step function, Θ, with respect to $\nabla_{\rm rad} - \nabla_{\rm ad}$, that is,

$$\nabla = \nabla_{\rm conv}\Theta(\nabla_{\rm rad} - \nabla_{\rm ad}) + \nabla_{\rm rad}\Theta(\nabla_{\rm ad} - \nabla_{\rm rad}). \tag{42}$$

However, introduction of the discontinuous function Θ induces a new numerical trouble. Therefore, we replace Θ with a suitable smooth function:

$$F(x) = \frac{1}{e^{\beta x} + 1}, \tag{43}$$

where

$$x = \nabla_{\rm rad} - \nabla_{\rm ad}. \tag{44}$$

Note that $F(x)$ varies with x smoothly and transits from 1 to 0 abruptly near $x = 0$: the width of the transition is nearly equal to β^{-1}. Though the numerical parameter β cannot be determined theoretically, it is confirmed that the choice of β has no great influence on the results of our calculations as long as we use $\beta \geq 1000$.

With the above-mentioned prescriptions, we can transform the basic differential equations, Eqs. (13), (14), (21), and (23), to ones suitable to our numerical calculation as follows:

$$\frac{\partial \ln P}{\partial M_r} = -\frac{GM_r}{4\pi r^4 P}, \tag{45}$$

$$\frac{\partial \ln r}{\partial M_r} = \frac{1}{4\pi r^3 \rho}, \tag{46}$$

$$\frac{\partial \ln T}{\partial M_r} = -\frac{GM_r}{4\pi r^4 P}\nabla, \tag{47}$$

and

$$L_r \frac{\partial \ln L_r}{\partial M_r} = \varepsilon_{\rm ac} - C_P T \left(\frac{d \ln T}{dt} - \nabla_{\rm ad} \frac{d \ln P}{dt} \right). \tag{48}$$

From Eqs. (42) - (44), it follows

$$\nabla = \nabla_{\rm conv} F(x) + \nabla_{\rm rad} F(-x). \tag{49}$$

Equation (48) requires a special comment because it contains time derivative. Writing Eq. (48) as $z = dy/dt$ for simplicity and designating quantities at $t = t^n$ and $t = t^n + \Delta t (\equiv t^{n+1})$ by superscripts n and $n+1$, respectively, we estimate the time derivative of y as

$$\frac{dy}{dt} = \frac{y^{n+1} - y^n}{\Delta t}. \tag{50}$$

On the other hand, we estimate z on the left hand side in a backward difference scheme, i.e.,

$$z = z^{n+1}. \tag{51}$$

From the viewpoint of numerical accuracy, it is better to adopt a time-centered scheme rather than the backward difference scheme. However, in the time-centered scheme, numerical time interval Δt is restricted absolutely

by the so-called *Courant condition* to guarantee the numerical stability. In our present problem, Δt has to be less than the time interval within which the thermal energy is transferred from one to another boundaries of each mass shell. As a result, Δt becomes too small (because of optical thinness near the outer boundary of the envelope) to accomplish numerical simulation of the protoplanetary evolution over the order of 1×10^7 yr. In the backward difference scheme, numerical instability never appears even if we adopt an arbitrarily large Δt. This is a reason why we adopt the backward difference scheme rather than the time-centered one.

3.2.2 Linearized Differential Equations

As described in §3.1, our main procedure is to find corrections by solving a set of linearized algebraic equations like Eq. (40). All the basic equations (Eqs. (45) - (48)) can be expressed in the form of

$$\frac{\partial \boldsymbol{X}}{\partial M_r} = \boldsymbol{A}, \tag{52}$$

where

$$\boldsymbol{X} = \begin{pmatrix} \ln r \\ \ln L_r \\ \ln P \\ \ln T \end{pmatrix} \tag{53}$$

and

$$\boldsymbol{A} = \begin{bmatrix} \dfrac{1}{4\pi r^3 \rho} \\ \varepsilon_{\rm ac} - C_P T \left(\dfrac{d \ln T}{dt} - \nabla_{\rm ad} \dfrac{d \ln P}{dt} \right) \\ -\dfrac{G M_r}{4\pi r^4 P} \\ -\dfrac{G M_r}{4\pi r^4 P} \nabla \end{bmatrix}. \tag{54}$$

Following the procedure mentioned in §3.1, we can readily obtain the linearized equation,

$$\sum_{k=1}^{4}\left(\frac{\partial \boldsymbol{A}}{\partial X_k}\right)^0 \delta X_k - \frac{\partial \delta \boldsymbol{X}}{\partial M_r} = \frac{\partial \boldsymbol{X}^0}{\partial M_r} - \boldsymbol{A}^0. \tag{55}$$

Now, we transform the differential equations (Eq. (55) at present) to the difference equations. For this purpose, we first divide the protoplanetary envelope into $J-1$ thin shells; the shell boundaries are labeled $1, 2, \cdots, J$ in the direction from the bottom of the envelope (the core surface) to the outer boundary. Let M_j be the mass contained within a sphere made by the j-th boundary. The quantity $\boldsymbol{X}$ is defined on the shell boundary and simply designated by the same subscript, i.e., $\boldsymbol{X}_j$.

Following Eq. (36), we obtain the difference equation for Eq. (55):

$$\frac{1}{2}\sum_{k=1}^{4}\left\{\left(\frac{\partial A}{\partial X_k}\right)^0_{j+1}\delta X_{k,j+1} + \left(\frac{\partial A}{\partial X_k}\right)^0_{j}\delta X_{k,j}\right\} + \frac{\delta \boldsymbol{X}_{j+1} - \delta \boldsymbol{X}_j}{\Delta M_{j+1/2}} = \frac{\boldsymbol{X}_{j+1} - \boldsymbol{X}_j}{\Delta M_{j+1/2}} - \frac{1}{2}(\boldsymbol{A}_{j+1} + \boldsymbol{A}_j) \tag{56}$$

for $j = 1, \cdots, J-1$, where

$$\Delta M_{j+1/2} = M_{j+1} - M_j. \tag{57}$$

As a result, we have $4J-4$ algebraic equations containing $4J$ unknown variables. Thus, we have to add 4 boundary conditions to a set of the equations presented above, according to Eqs. (26) and (27). Equation (56) is solved with the help of the matrix-inversion method. As seen from Eq. (56), each algebraic equation needs only information of two adjacent shell boundaries. This makes the problem significantly easy, because the matrix becomes a simple band-matrix.

3.3 Gas Accretion Rate

The total mass of the protoplanet, $M_{\rm t}$, increases with time according to Eq. (25):

$$\frac{dM_{\rm t}}{dt} = 4\pi R^2 \rho_0 \left(\frac{dR}{dt} - V \right) + \dot{M}_{\rm c}. \tag{58}$$

This equation also has to be transformed into the difference equation in the similar manner used in the previous subsection. Approximating as

$$V = \frac{r_J^{n+1} - r_J^n}{\Delta t}, \tag{59}$$

we have the difference form of Eq. (58),

$$M_{\rm t}^{n+1} - M_{\rm t}^n = 4\pi \left(R^{n+1} \right)^2 \rho_0 \left(R^{n+1} - r_{\rm J}^{n+1} \right) + \dot{M}_{\rm c} \Delta t, \tag{60}$$

where we have used the relation, $r_J^n = R^n$. Note that r_J^{n+1} is not equal to R^{n+1}. That is, r_J^{n+1} is only the radius of the outermost mass shell at t^{n+1} (usually $r_J^{n+1} < r_J^n$), which is calculated in the manner described in the previous section. On the other hand, R^{n+1} is the planetary radius at t^{n+1} (usually $R^{n+1} > r_J^n$), which is determined by the planetary mass and/or the sound velocity of the nebular gas (see Eqs. (8) and (9)).

Letting

$$M_{\rm t}^{n+1} = M_{\rm t}^0 + \delta M_{\rm t}, \qquad R^{n+1} = R^0 + \delta R, \quad \text{and} \quad r_J^{n+1} = r_J^0 + \delta r_J, \tag{61}$$

substituting Eq. (61) into Eq. (60), and neglecting the second and higher order terms, we obtain the linearized equation for Eq. (60):

$$M_{\rm t}^0 + \delta M_{\rm t} - M_{\rm t}^n = 4\pi \left(R^0 \right)^2 \rho_0 \left\{ R^0 - r_J^0 + \left(3 - \frac{2r_J^0}{R^0} \right) \delta R - \delta r_J \right\} + \dot{M}_{\rm c} \Delta t. \tag{62}$$

Here, the number of unknown variables is not three but two, because $\delta M_{\rm t}$ and δR are related by Eq. (9). Putting $M_{\rm t}^0$ equal to be $M_{\rm t}^n$ and solving the structure equations in the manner described in the previous section, we obtain the variation δr_J of the radius of the previous outermost mass shell. Substituting it into Eq. (62), we have the increment $\delta M_{\rm t}$ of the total mass of the protoplanet. This process is repeated until the variation δR becomes sufficiently small.

Finally, prior to the numerical simulations of the quasi-static evolution of the protoplanetary envelope, we have to give an initial model. Initial models are constructed by the integration method which is identical to that used by Mizuno (1980). The method is described in the next subsection.

3.4 Method for Finding the Critical Core Mass

As mentioned at the beginning of this section, the critical core mass and the luminosity at the critical core mass, which are obtained with the help of the static calculation, give us very important information. In this subsection, we describe the method for finding the critical core mass.

The static calculation requires the assumption that the envelope is in thermal equilibrium, that is, the typical evolutionary time of the envelope is longer than the thermal relaxation time. Under this assumption, we can set $TdS/dt = 0$ in Eq. (23), so that we have

$$L_r = L_{\rm ac} (= \text{constant}), \tag{63}$$

where

$$L_{\rm ac} = \int_0^R 4\pi r'^2 \rho \varepsilon_{\rm ac} dr'. \tag{64}$$

If we know the value of $L_{\rm ac}$, we can obtained an equilibrium solution of the envelope structure for a given core mass by solving Eqs. (13), (14), and (21) with the boundary conditions Eqs. (26) and (27) excluding that for L_r. Certainly, we might be able to find the solutions with the above-mentioned relaxation method, but more easy way is the inward integration method.

For a given planetary mass $M_{\rm t}$, we can know the planetary radius (see Eq. (9)) and the density and the temperature at $M_r = M_{\rm t}$. Based on these values and giving a trial value of $L_{\rm ac}$, we integrate Eqs. (13), (14), and (21) inwards with the 4th-order Runge-Kutta method. We continue the integration to the point where the mean density interior to the point is equal to the presumed mean density of the core and, as a result, we can obtain the mass of the core. Then, we calculate $L_{\rm ac}$ using the obtained density distribution and Eq. (64). The newly obtained $L_{\rm ac}$ does not always coincide with the previously assigned $L_{\rm ac}$. In this case, we select a new $L_{\rm ac}$ and perform the same procedure again. We continue this procedure until we find $L_{\rm ac}$ within the desired accuracy (Mizuno 1980).

By performing the above-mentioned procedures for various planetary total masses, we can obtain the relation between the core mass and the planetary total mass. As shown by Mizuno (1980), the relation has a maximum value of the core mass, beyond which no equilibrium solution can be found. This maximum core mass is the critical core mass (see Fig. 9).

4 Formation of the Massive Envelope: Dependences on Various Parameters

In this section, we investigate the dependence of the accretion time of the envelope as well as that of the critical core mass on the five parameters included in the nucleated instability model; the parameters are core accretion rate, grain opacity (or, the grain depletion factor), density and temperature of the nebular gas, and distance from the central star. As mentioned in §1.4, all the parameters are not always important. That is, when the envelope is radiative (strictly speaking, partially convective), the parameters, which govern the outer boundary conditions of the envelope, are not important (Mizuno 1980; Stevenson 1982b). On the other hand, in the case where the envelope is wholly convective, the core accretion rate and the grain opacity are not important, because they play a significant role only in the radiative transfer. Thus, we can classify the parameters into two groups: one includes the core accretion rate and the grain opacity and the other includes the density and temperature of the nebular gas and the distance from the central star.

In §4.1, we investigate the dependences on the core accretion rate and the grain opacity. In this study, we assume that the protoplanet is located at 5.2 AU in the minimum-mass solar nebula. First, we see the critical core mass over a wide range of the core accretion rate and the grain depletion factor (§4.1.1). Next, we present the quasi-static evolution of the envelope in the two extreme cases, the case where the core accretion is halted abruptly (§4.1.2) and the case where the core accretion continues steadily (§4.1.3). Finally, we derive a semi-analytical expression for the accretion time of the envelope

as a function of the critical core mass and the grain depletion factor, which agrees well with our results of quasi-static calculations (§4.1.4). Furthermore, we investigate the dependences of the critical core mass on the boundary conditions of the envelope in §4.2: the density and temperature of the nebular gas in §4.2.2 and the distance from the central star in §4.2.3.

4.1 Core Accretion Rate and Grain Opacity - Partially Convective Envelope -

4.1.1 Critical Core Mass and Critical Luminosity

In Fig. 2a, we show the calculated critical core mass, $M_c^{\rm crit}$, as a function of the core accretion rate, $\dot{M}_c$, for typical five values of the grain depletion factor, f. As seen from Fig. 2a, $M_c^{\rm crit}$ decreases with decreases both in $\dot{M}_c$ and in f. Especially, $M_c^{\rm crit}$ is as small as $0.3M_\oplus$ when $\dot{M}_c < 1 \times 10^{-11} M_\oplus/{\rm yr}$ and $f < 1 \times 10^{-2}$. Even a very small core has the ability to capture the nebular gas. Roughly speaking, $M_c^{\rm crit}$ depends on $\dot{M}_c$ and f as

$$M_c^{\rm crit} \propto \left(\dot{M}_c f\right)^{0.2-0.3}. \tag{65}$$

Note that our results for $\dot{M}_c = 1 \times 10^{-6} M_\oplus/{\rm yr}$ are larger by a factor of about 2 than those given by Mizuno (1980), mainly because the grain opacity used here is larger than that he used (see §2.4).

For our later convenience, we introduce *the critical luminosity*, $L^{\rm crit}$, which is defined as the energy release rate by incoming planetesimals when $M_c = M_c^{\rm crit}$. In other words, the critical luminosity is the minimum energy input rate for the envelope to be sustained in hydrostatic equilibrium without the help of the gravitational energy release caused by contraction of the envelope itself. It will be seen later that the critical luminosity plays an important

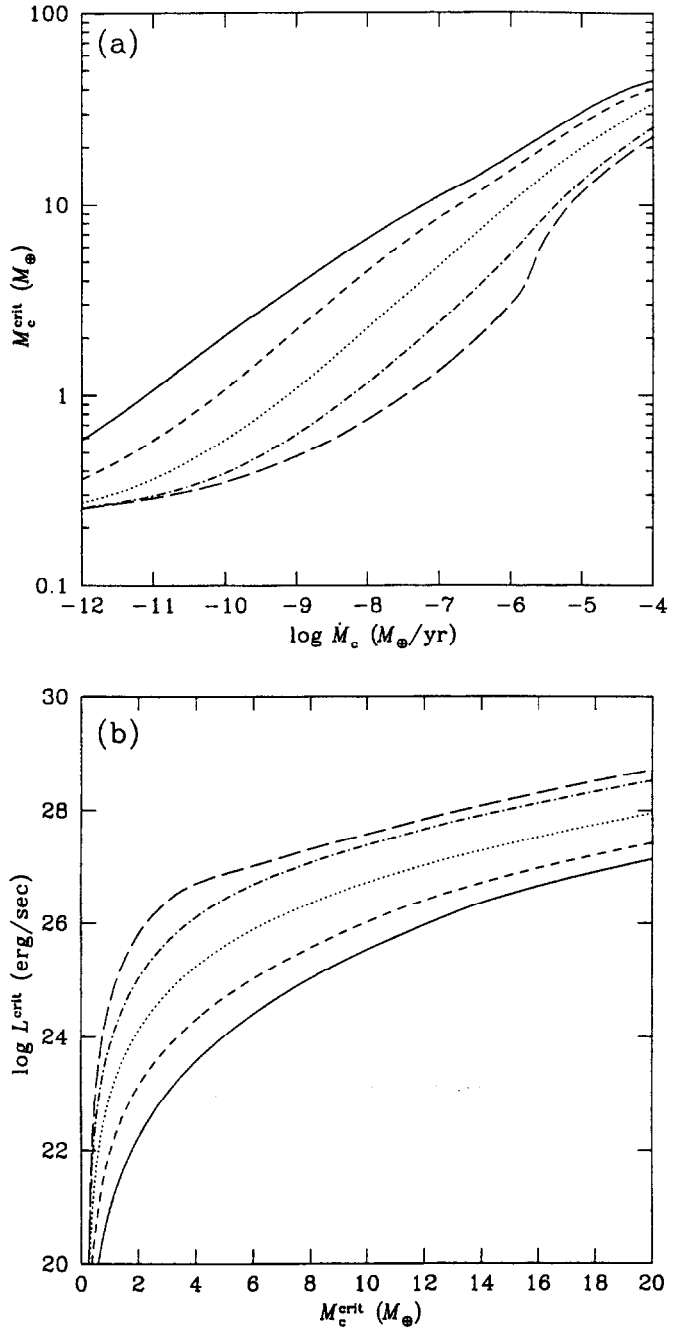

Figure 2: The critical core mass, $M_c^{\rm crit}$, as a function of the core accretion rate, $\dot{M}_c$, (Fig. (a)) and the critical luminosity, $L^{\rm crit}$, as a function of the critical core mass, $M_c^{\rm crit}$, (Fig. (b)) for $f = 1$ (*solid line*), 1×10^{-1} (*short dashed line*), 1×10^{-2} (*dotted line*), 1×10^{-3} (*dot-dashed line*), and 1×10^{-4} (*long dashed line*).

role in analyzing the quasi-static evolution of the envelope. The critical luminosity evaluated numerically is shown in Fig. 2b as a function of $M_{\rm c}^{\rm crit}$ for five f's. As we can readily understand, $L^{\rm crit}$ is smaller for smaller $M_{\rm c}^{\rm crit}$ and larger for smaller f. Note that $L^{\rm crit}$ depends strongly on $M_{\rm c}^{\rm crit}$:

$$L^{\rm crit} \propto (M_{\rm c}^{\rm crit})^{4-5} f^{-1}. \tag{66}$$

It should be mentioned that the critical luminosities obtained in this study are about 10 times as small as those given by Ikoma *et al.* (2000). The difference becomes large, as the critical core mass decreases. This is because our grain opacity is larger by a factor of 10 to 20 than that used by them and the critical luminosity is inversely proportional to the grain opacity (see Eq. (66)). Furthermore, the envelope structure becomes more centrally condensed one, as the luminosity decreases (thereby, the critical core mass decreases). In other words, the density at a given temperature becomes high, as the luminosity decreases. As we can understand from Fig. 1, as the density becomes high, the grain opacity becomes large, because each evaporation temperature of each species increases. This is why the differences between Ikoma *et al.* (2000)'s results and ours become large, as the critical core mass decrease.

4.1.2 Evolution in the Case of Isolation from Planetesimals

As mentioned in §1.2.1, most of the giant planets may have been isolated from planetesimals, before their core masses reached the conventional critical core mass ($\sim 10 M_\oplus$). Then, core accretion halted and no energy was supplied by planetesimals. Afterward, the envelope contracted gravitationally and the surrounding nebular gas accreted onto the envelope. In this subsubsection,

we study how long it takes for the core to capture the surrounding nebular gas after the core accretion has stopped (i.e., $t \geq t_0$ in Eq. (32)).

Figure 3a shows a typical example of evolution of the envelope mass, $M_{\rm env}$, after core accretion is halted in the case where $M_{\rm c} = 5M_\oplus$ and $f = 1$ (note that we have designated $\dot{M}_{\rm c}^0 t_0$ simply as $M_{\rm c}$). Initially, $M_{\rm env} = 1.3 \times 10^{-2} M_\oplus$. A halt of the core accretion triggers sudden gas accretion, so that $M_{\rm env}$ increases by a factor of 10 in 2.0×10^5yr. However, the accretion rate of the envelope decreases increasingly; a further increase in $M_{\rm env}$ by a factor of 10 takes 2.7×10^7yr and the next increase by a factor of 10 requires no less than 1.3×10^8yr. Afterward, the gas accretion is rapidly accelerated. The envelope spends most of its evolutionary time in the intermediate phase, where the envelope mass increases moderately, after the core accretion has stopped. The luminosity, L, which is shown in Fig. 3b, evolves correspondingly to the evolution of $M_{\rm env}$. It is relatively high at the initial stage ($L = 3.5 \times 10^{26}$erg/sec) but decreases rapidly after the core accretion is stopped and reaches its minimum value, $L_{\rm min}$ ($= 1.9 \times 10^{24}$erg/sec) at $t - t_0 = 5.0 \times 10^7$yr. Afterward, the luminosity increases gradually until $t - t_0 = 1.3 \times 10^8$yr and rapidly after $t - t_0 = 1.3 \times 10^8$yr. The luminosity stays near the level of $L_{\rm min}$ during the phase corresponding to the intermediate phase above mentioned.

Since the total evolutionary time is almost equal to the duration of the intermediate phase in which $L \simeq L_{\rm min}$, the characteristic growth time of the envelope mass, $\tau_{\rm g}^0$, is given by

$$\tau_{\rm g}^0 \equiv \left(\frac{1}{M_{\rm env}} \frac{dM_{\rm env}}{dt} \right)^{-1}_{L=L_{\rm min}}, \tag{67}$$

where the subscript $_{L=L_{\rm min}}$ means that the derivative is evaluated at $L = L_{\rm min}$ (i.e., $t - t_0 = 5.0 \times 10^7$yr in the case of Fig. 3a). In Tables 1 and 2, we tabulate

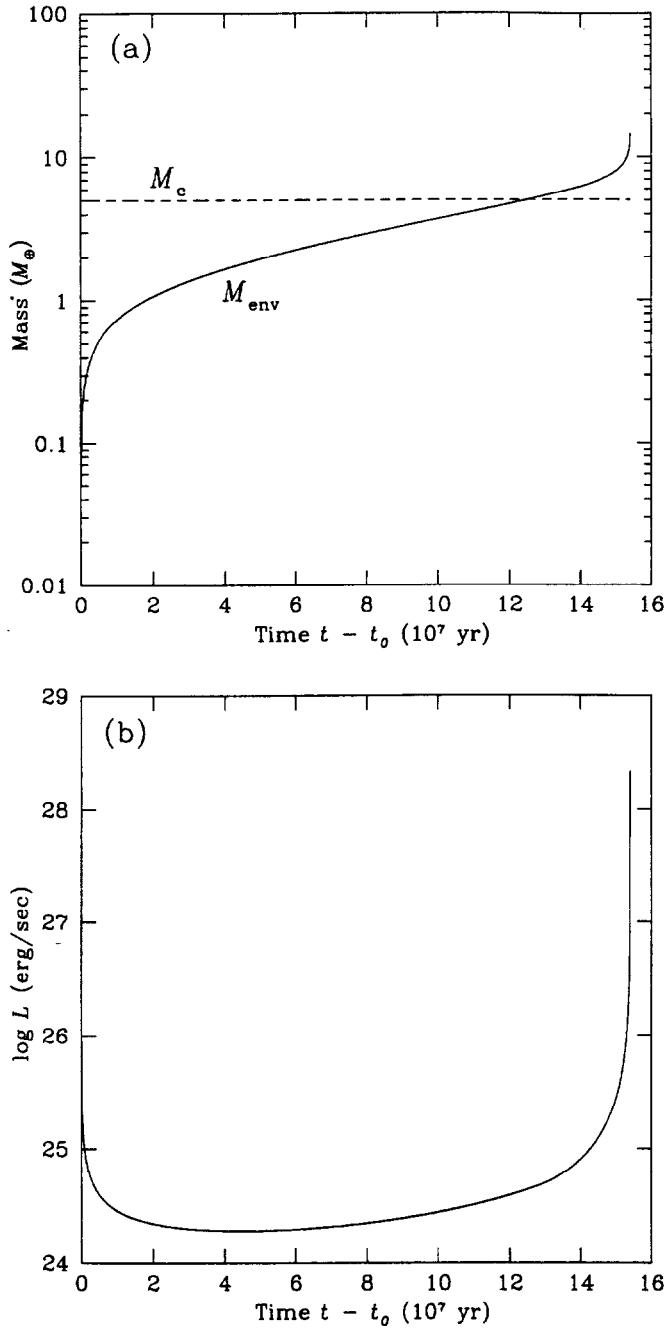

Figure 3: A typical example of evolution of the envelope after core accretion is halted in the case of $M_c = 5M_\oplus$ and $f = 1$. Figure (a) shows the envelope mass, M_{env}, (*solid line*) and the core mass, M_c, (*dashed line*) and Fig. (b) presents the luminosity, L.

Table 1: Growth time, τ_g^0, in the case of $\tau_d \to 0$ ($f = 1$)

$M_c(M_\oplus)$	τ_g^0(yr)
3	3.2×10^8
4	1.3×10^8
5	6.2×10^7
6	3.2×10^7
8	1.0×10^7
10	4.1×10^6

Table 2: Growth time, τ_g^0, in the case of $\tau_d \to 0$ ($M_c = 5M_\oplus$)

f	τ_g^0(yr)
1	6.2×10^7
1×10^{-1}	6.0×10^6
1×10^{-2}	5.0×10^5

τ_g^0 evaluated from our numerical simulations for six values of M_c with $f = 1$ and for three values of f with $M_c = 5M_\oplus$, respectively. Table 1 shows that τ_g^0 increases rapidly with decreasing M_c: for example, $\tau_g^0 = 3.2 \times 10^7$yr for $M_c = 6M_\oplus$, whereas $\tau_g^0 = 3.2 \times 10^8$yr for $M_c = 3M_\oplus$. On the other hand, as seen from Table 2, τ_g^0 depends moderately on f (τ_g^0 being almost linearly proportional to f). Here, we should mention that each value of τ_g^0 is also 10 times as large as that given by Ikoma *et al.* (2000).

Figure 4 shows $L_{\rm min}$ as a function of M_c together with the critical luminosity multiplied by 2, i.e., $2L^{\rm crit}$. As seen from Fig. 4, $L_{\rm min}$ increases with increasing M_c and decreasing f. Furthermore, it is interesting to note that $L_{\rm min}$ is almost equal to $2L^{\rm crit}$. The critical luminosity, $L^{\rm crit}$, is the minimum luminosity to support the envelope around a core with mass of M_c. Hence,

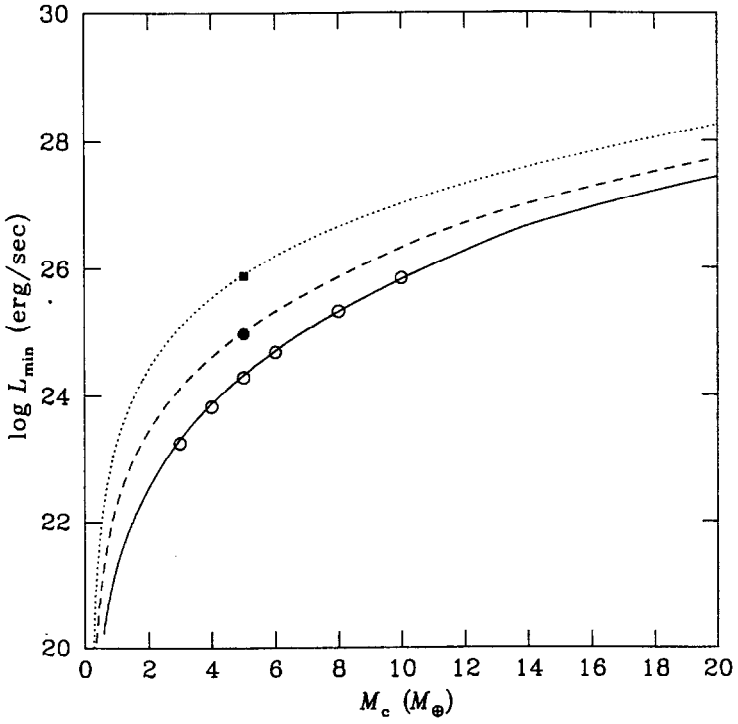

Figure 4: The minimum luminosity, $L_{\rm min}$, as a function of the core mass, $M_{\rm c}$. The open circles, the filled circle, and the filled square show $L_{\rm min}$ found numerically for $f = 1, 0.1$, and 0.01, respectively. The critical luminosity, $L^{\rm crit}$, multiplied by 2 is also plotted for $f = 1$ (*solid line*), 0.1 (*dashed line*), and 0.01 (*dotted line*).

$L^{\rm crit}$ should be $\sim L_{\rm min}$. The numerical factor (~ 2) arises from the difference in spatial distribution of energy sources. The energy supply caused by planetesimals (corresponding to $L^{\rm crit}$) is confined very near the bottom of the envelope, whereas the energy source caused by the contraction (corresponding to $L_{\rm min}$) is distributed throughout the envelope. Since the former supports the envelope more efficiently, $L_{\rm min} > L^{\rm crit}$. Despite the fact that the distributions of the two energy sources are very different from each other, the effect is so small that it yields only small difference (i.e., a factor of 2)

between $L_{\rm min}$ and $L^{\rm crit}$. This is because convection usually occurs in the inner envelope, the structure of which is determined independently of the distribution of the energy source and, furthermore, the mass of the convective region occupies a large fraction of the envelope mass.

4.1.3 Evolution in the Case of Steady Core Accretion

In the previous subsection, we considered the case in which growth of a core stopped completely because of the isolation from planetesimals (i.e., the case of $\tau_{\rm d} \to 0$). In the actual planetary formation, however, the growth of the core would not halt suddenly but its rate would decrease gradually, that is, $\tau_{\rm d}$ would be finite. To know how the growth time of the envelope mass depends on $\tau_{\rm d}$, we consider another extreme case, namely, the case of $\tau_{\rm d} \to \infty$ in this subsection.

Figure 5a shows time-variation of $M_{\rm c}$ and $M_{\rm env}$ for $\dot{M}_{\rm c}^0 = 1 \times 10^{-6} M_\oplus/{\rm yr}$ and $f = 1$ (initially $M_{\rm c} = 0.1 M_\oplus$). As seen from this figure, the envelope mass increases gradually until the core mass reaches about $20 M_\oplus$, which is almost equal to the critical core mass obtained by the static calculation (see Fig. 2a). After that, the envelope mass increases much more rapidly than the core mass. Unlike the case of $\tau_{\rm d} \to 0$, both the core mass and the envelope mass grow in the case of $\tau_{\rm d} \to \infty$, as a matter of course. Since we are now interested in the phase where the envelope mass increases much more rapidly than the core mass, we focus particular attention on the latter phase. As we will show below, the energy release due to contraction of the envelope is not important compared to that by planetesimals in the former phase and, therefore, the evolutionary behavior of the protoplanet in the former phase can be known without the help of quasi-static calculation if $\dot{M}_{\rm c}(t)$ is given

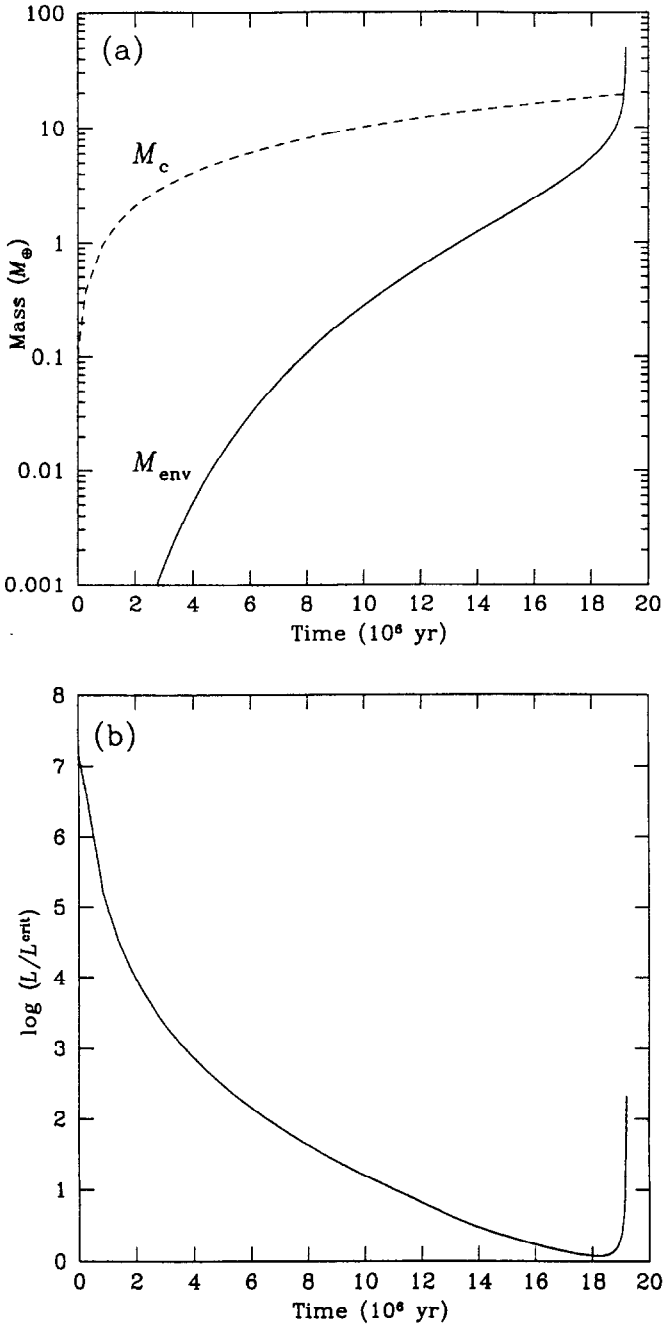

Figure 5: A typical example of evolution of the envelope in the case where $\dot{M}_c^0 = 1 \times 10^{-6} M_\oplus/\mathrm{yr}$, $\tau_d \to \infty$, and $f = 1$. Figure (a) shows the envelope mass, M_{env}, (*solid line*) and the core mass, M_c, (*dashed line*) and Fig. (b) presents the luminosity, L, normalized by the critical luminosity, L^{crit}.

by the theory of planetary accretion.

As shown in the previous subsection, we should see the evolutionary behavior of the luminosity to understand that of the envelope mass. To define the transition point from the former phase to the latter one exactly, we introduce the following normalized luminosity:

$$\tilde{L} = L/L^{\rm crit}, \tag{68}$$

where $L^{\rm crit}$ is the critical luminosity shown in Fig. 2b (note that Fig. 3b does not change with the use of $\tilde{L}$ instead of L except the scale of the vertical axis). Figure 5b shows the normalized luminosity as a function of time. In the early stage, $\tilde{L}$ is very large, which means that the energy supplied by incoming planetesimals is large enough for the envelope to be maintained in hydrostatic equilibrium. However, $\tilde{L}$ decreases with time because $L^{\rm crit}$ increases with increasing $M_{\rm c}$. When $\tilde{L}$ reaches the minimum value, $\tilde{L}_{\rm min}(\sim 1)$, the envelope cannot be supported only by the energy supply caused by planetesimals any more, so the envelope stars to contract in order to supply extra energy. As a result, $\tilde{L}$ begins to increase rapidly. We are now interested in the growth time of the envelope mass at $\tilde{L} = \tilde{L}_{\rm min}$, because the growth time at $\tilde{L} = \tilde{L}_{\rm min}$ is longest in the latter phase.

Table 3 shows the core mass, $M_{\rm c}$, at $\tilde{L} = \tilde{L}_{\rm min}$ and the characteristic growth time, $\tau_{\rm g}^{\infty}$, the definition of which is similar to that of $\tau_{\rm g}^{0}$, i.e.,

$$\tau_{\rm g}^{\infty} \equiv \left(\frac{1}{M_{\rm env}} \frac{dM_{\rm env}}{dt} \right)^{-1}_{\tilde{L}=\tilde{L}_{\rm min}}. \tag{69}$$

As seen from this table, $M_{\rm c}$ at $\tilde{L} = \tilde{L}_{\rm min}$ is smaller for smaller $\dot{M}_{\rm c}^{0}$. Each of them is almost equal to each $M_{\rm c}^{\rm crit}$ as seen from Fig. 2a. The growth time of the envelope mass, $\tau_{\rm g}^{\infty}$, is larger for smaller $\dot{M}_{\rm c}^{0}$, i.e., smaller $M_{\rm c}$.

Table 3: Growth time, $\tau_{\rm g}^{\infty}$, and core mass, $M_{\rm c}$, when $\tilde{L} = \tilde{L}_{\rm min}$ in the case of $\tau_{\rm d} \to \infty$ ($f = 1$)

$\dot{M}_{\rm c}^{0}(M_{\oplus}/{\rm yr})$	$M_{\rm c}(M_{\oplus})$	$\tau_{\rm g}^{0}({\rm yr})$
1×10^{-9}	4.0	4.5×10^{8}
1×10^{-8}	6.9	7.4×10^{7}
1×10^{-7}	11	1.1×10^{7}
1×10^{-6}	18	1.7×10^{6}

This tendency is the same as that found in the case of $\tau_{\rm d} \to 0$. Furthermore, comparing $\tau_{\rm g}^{0}$ in Table 1 and $\tau_{\rm g}^{\infty}$ in Table 3 for $M_{\rm c} = 4.0 M_{\oplus}$, we can find that both are of the same order of magnitude, although $\tau_{\rm g}^{\infty}$ is somewhat larger than $\tau_{\rm g}^{0}$.

4.1.4 Growth Time of the Envelope Mass

In this subsection, we derive an expression for the characteristic growth time of the envelope mass through semi-analytical arguments.

Gas accretion is regulated by contraction of the outer envelope. The growth time of the envelope mass is, therefore, described by the characteristic time of the contraction. The characteristic time of the contraction is determined by the amount of supplied energy and the efficiency of the energy transfer, i.e., the luminosity. In the absence of planetesimal accretion, the only energy source is the gravitational energy of the envelope and, hence, the characteristic time of the contraction should be written as

$$\frac{G M_{\rm c} M_{\rm env}}{\mathcal{R}\mathcal{L}}, \tag{70}$$

where $\mathcal{R}$ is an effective radius beyond which significant contraction occurs with an appreciable energy release. From our results in §§4.1.2 and 4.1.3,

we should take $L^{\rm crit}$ (which is given in Fig. 2b) as the characteristic luminosity, $\mathcal{L}$, and the critical envelope mass, $M_{\rm env}^{\rm crit}$ (which is the envelope mass at $M_{\rm c} = M_{\rm c}^{\rm crit}$) as $M_{\rm env}$ in Eq. (70). Furthermore, the radius, $\mathcal{R}$, should be not the core radius $r_{\rm c}$ but the radius of the boundary between convective and radiative regions, $R_{\rm conv}$, because the envelope is usually composed of an inner convective region and an outer radiative region and considerable contraction occurs in the radiative region. Thus, the growth time, $\tau_{\rm g}$, which is an analytical expression for $\tau_{\rm g}^0$ (or $\tau_{\rm g}^\infty$) in the case of $\tau_{\rm d} \to 0$ (or $\tau_{\rm d} \to \infty$), can be written in the form,

$$\tau_{\rm g} = \alpha \frac{G M_{\rm c} M_{\rm env}^{\rm crit}}{R_{\rm conv} L^{\rm crit}}. \tag{71}$$

A numerical coefficient, α, depends on the detailed structure of the envelope and is determined by comparison with the numerical results.

In Fig. 6a, we show $\tau_{\rm g}$ evaluated by substituting our hydrostatic solutions into Eq. (71) (with $\alpha = 1/3$) together with $\tau_{\rm g}^0$ found by our quasi-static simulations in the case where $\tau_{\rm d} \to 0$. This figure shows that $\tau_{\rm g}$ with $\alpha = 1/3$ agrees well with $\tau_{\rm g}^0$. It takes longer time for the smaller core to capture a massive envelope; roughly speaking, $\tau_{\rm g}$ is written as

$$\tau_{\rm g} \sim 1 \times 10^{10} f \left(\frac{M_{\rm c}}{M_\oplus} \right)^{-3.5} \ {\rm yr}. \tag{72}$$

From this equation, it follows that there exists a minimum core mass to form the massive envelope within the lifetime of the nebula. The quantitative discussion will be made in §5.

We should be mentioned that both the absolute value of $\tau_{\rm g}$ and its dependence on $M_{\rm c}$ obtained in this study are quite different from those by Ikoma *et al.* (2000). In particular, $\tau_{\rm g}$ for $M_{\rm c} = 1 M_\oplus$ in this study is more than

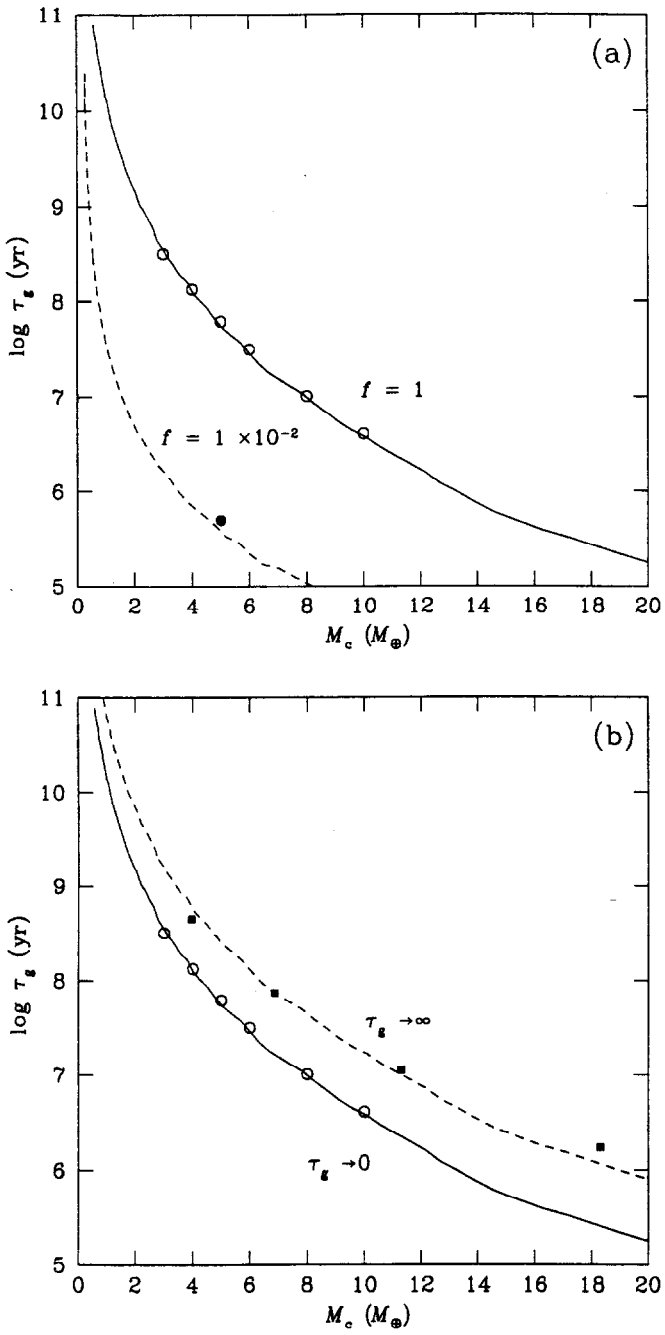

Figure 6: (a) The growth time, τ_g, as a function of the core mass, M_c, in the case of $\tau_d \to 0$. The solid (for $f = 1$) and dashed (for $f = 0.01$) lines represent τ_g obtained from Eq. (71) with $\alpha = 1/3$. Circles show the corresponding growth times, τ_g^0, found from our quasi-static calculations. (b) τ_g for $\tau_d \to 0$ (*solid line*) and $\tau_d \to \infty$ (*dotted line*). Circles and squares represent τ_g^0 and τ_g^∞, respectively.

10 times as large as that given by Ikoma *et al.* (2000). This stems not only from the fact that our grain opacity is larger by a factor of 10 to 20 than that used by them, but also that the discrepancy between their results and ours becomes larger, as the core mass decreases (see §4.1.1).

As shown in Fig. 6b, τ_g evaluated by Eq. (71) with $\alpha = 3/2$ (*dotted line*) also agrees well with τ_g^{∞}. The growth time, τ_g, in the case of $\tau_d \to \infty$ is about 4 - 5 times as large as that in the case of $\tau_d \to 0$. This is because, in the case of $\tau_d \to \infty$, the energy of the envelope is supplied partly by incoming planetesimals. The difference is no more than a factor of 4 - 5 even between the two extreme cases, i.e., $\tau_d \to 0$ and $\tau_d \to \infty$. Therefore, we can conclude that τ_g depends on τ_d only weakly.

Finally, we make a short comment on the influence of the initial core accretion rate, $\dot{M}_c^0$, in the case of $\tau_d \to 0$. Although $\dot{M}_c^0$ directly influences the evolutionary time in the early stage, during which the luminosity decreases from the initial value to $L_{\rm min}$, this period is much shorter than that of the phase of $L \simeq L_{\rm min}$. Also, the characteristic growth time of the envelope mass at $L = L_{\rm min}$ is determined completely by the critical luminosity and the corresponding quantities (without any information of the initial values). Hence, our results do not depend on the choice of $\dot{M}_c^0$.

4.1.5 Summary of Dependences on Core Accretion Rate and Grain Opacity

In summary, we have obtained the following results in this subsection.

1. Considerable gas accretion necessarily begins, independently of the past core accretion process, when the luminosity becomes almost equal to the critical luminosity (which is given in Fig. 2b), whether the lumi-

nosity originates in incoming planetesimals or the contraction of the envelope. Even a core with about the Martian mass can start to capture the surrounding nebular gas if the luminosity and the opacity are sufficiently small.

2. There exists an intermediate phase characterized by a moderate increase in the envelope mass after core accretion is halted. The duration of this phase occupies a large fraction of the formation time of the massive envelope.

3. The characteristic growth time of the envelope mass, $\tau_{\rm g}$, (which is almost equal to the duration of the intermediate phase) depends strongly on the core mass, moderately on the grain opacity, and weakly on the past core accretion process; roughly speaking, $\tau_{\rm g}$ is written in the form of

$$\tau_{\rm g} \sim 1 \times 10^{10} f \left(\frac{M_{\rm c}}{M_\oplus} \right)^{-3.5} \ {\rm yr}. \tag{73}$$

Result 3 suggests that there exists the minimum core mass in the sense that the core with mass less than this minimum mass is unable to capture a large amount of the nebular gas within its lifetime.

It may be worthwhile to compare the intermediate phase (Result 2) with Phase 2, which was found by Pollack *et al.* (1996). These two phases resemble each other, but differ from each other because there still exists the energy supply caused by incoming planetesimals in Phase 2. Pollack *et al.* (1996) suggested that a moderate increase in the envelope mass during Phase 2 originated in further accretion of planetesimals because of the extension of the

feeding zone of a protoplanet; thus, the elapsed time of Phase 2 was governed by the later core accretion process. On the other hand, we have shown that there exists a phase of a moderate increase in the envelope mass even if core accretion is halted and the characteristic growth time is determined by the contraction of the envelope. Thus, it is natural to consider that the physical essence of Phase 2 is the contraction of the envelope partly sustained by the energy caused by planetesimal accretion. Our obtained elapsed time gives the minimum elapsed time of Phase 2.

4.2 Properties of the Nebula - Wholly Convective Envelope -

4.2.1 Possibility of the Convective Envelope

As mentioned in §1.3.1, it is well known that, in the case where the outer envelope is radiative, the critical core mass scarcely depends on the outer boundary conditions of the envelope, i.e., distance from the central star and the density and temperature of the nebular gas. This is because envelope solutions with different boundary conditions soon converge in the radiative region near the surface of the envelope (Mizuno 1980; Stevenson 1982b). However, when the envelope is convective, the critical core mass generally depends on the outer boundary conditions, as pointed out by Wuchterl (1993).

In a chemically homogeneous hydrostatic envelope, the condition for the convective instability is given by Eq. (20):

$$\frac{3}{64\pi\sigma_{\rm SB}G}\frac{\kappa L_r}{M_r}\frac{P}{T^4} > 1-\frac{1}{\Gamma_2}, \tag{74}$$

where Γ_2 is the second adiabatic exponent and we used the relation $\nabla_{\rm ad} =$

$1-\Gamma_2^{-1}$. Since the thermal energy is supplied to the envelope by incoming planetesimals until the core mass reaches the critical core mass, L_r/M_r in Eq. (74) can be approximately written in the form of

$$\frac{L_r}{M_r} \simeq \left(\frac{4\pi\rho_c}{3}\right)^{1/3} \frac{G\dot{M}_c}{M_c^{1/3}}. \tag{75}$$

By substituting Eq. (75) into Eq. (74) and using the equation of state for an ideal gas, we can rewrite Eq. (74) in terms of the density, ρ, as

$$\rho > \frac{64\pi\sigma_{SB}\mu m_H \left(1-\Gamma_2^{-1}\right)}{3k\left(4\pi\rho_c/3\right)^{1/3}} \frac{M_c^{1/3}T^3}{\kappa\dot{M}_c}, \tag{76}$$

where k, μ, and m_H are the Boltzmann constant, the mean molecular weight, and the mass of a hydrogen atom, respectively. Substituting typical values characterizing the surface of the envelope into Eq. (76) and assuming that $\mu = 2.3$, $\Gamma_2 = 7/5$, and $\rho_c = 5.5\mathrm{gcm}^{-3}$, we obtain the critical nebular density, $\rho_{0,cr}^{surf}$, beyond which convection occurs near the surface:

$$\frac{\rho_{0,cr}^{surf}}{\rho_0^H} \simeq 5\left(\frac{a}{1\mathrm{AU}}\right)^{5/4}\left(\frac{T_0}{T_0^H}\right)^3\left(\frac{M_c}{20M_\oplus}\right)^{1/3}\left(\frac{\kappa}{1\mathrm{cm}^2\mathrm{g}^{-1}}\right)^{-1}\left(\frac{\dot{M}_c}{10^{-6}M_\oplus\mathrm{yr}^{-1}}\right)^{-1}, \tag{77}$$

where ρ_0^H is the density given by the minimum-mass solar nebula (see Eq. (29)). From Eq. (77), we see that, if the nebula is dense and/or cool compared to the minimum mass solar nebula or if the semimajor axis is smaller than about 1AU, convection can occur near the surface of the envelope. That is, the critical core mass is expected to depend on the boundary conditions in the regions where the extrasolar planets exist.

As described in §1.2.4, the recent observations suggest that there exist dense nebulae that are about 10 times as massive as the minimum-mass solar

nebula. On the other hand, theoretical models of structure of an optically thick, passive nebula (Chiang and Goldreich 1997; Sasselov and Lecar 2000 and references therein) indicate that the nebular temperature is lower than that given by the minimum-mass solar nebula model (see §2.3). Thus, it is very meaningful to consider a dense and cool nebula as a planet-forming nebula.

We should mention that Wuchterl (1993) derived an asymptotic expression for the critical core mass under the assumption of a wholly convective envelope with a constant adiabatic exponent. However, we cannot evaluate the precise values of the critical core mass from his expression, because the expression fails in representing his numerical results.

In our numerical calculations, we adopt $1 \times 10^{-6} M_{\oplus} \mathrm{yr}^{-1}$ as the core accretion rate and the interstellar one as the grain opacity for comparison with Wuchterl (1993). Our nominal values of the nebular density and temperature are those of the minimum-mass solar nebula model given by Eqs. (29) and (30) and we investigate the critical core mass over a wide range of the nebular density normalized by ρ_0^{H} at several distances from the central star for some typical temperatures.

4.2.2 Density and Temperature of the Nebular Gas

In Fig. 7, the critical core mass, $M_{\mathrm{c}}^{\mathrm{crit}}$, at 0.1AU is illustrated as a function of the nebular density (normalized by ρ_0^{H}) for the case of $T_0 = 885\mathrm{K}$, which is equal to T_0^{H} (*solid line*). For comparison, we also show the result calculated in the case where we set the envelope wholly convective artificially (*dashed line*). When the nebular density is low (i.e., $\rho_0 \lesssim 10\rho_0^{\mathrm{H}}$), the solid line lies below the dashed one and the critical core mass represented by the solid line is nearly

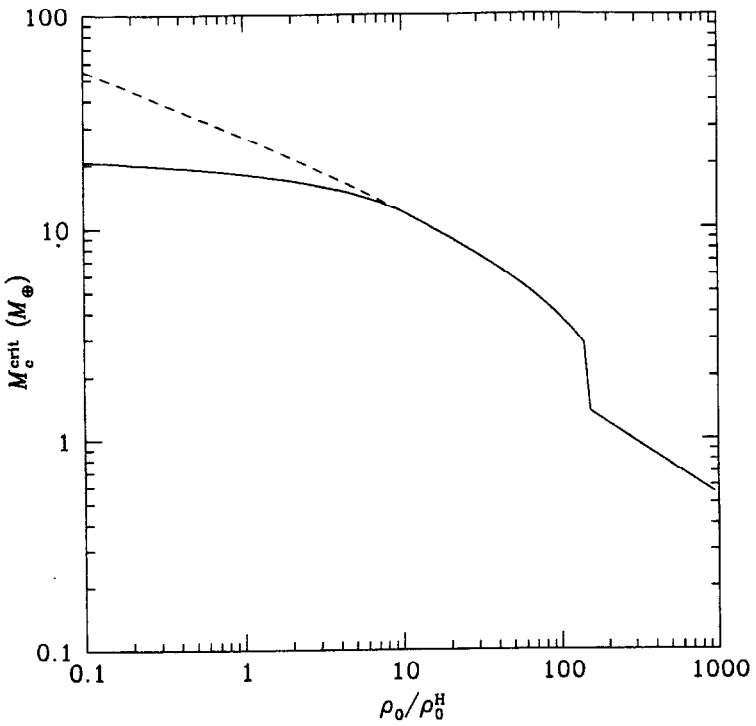

Figure 7: The critical core mass, M_c^{crit}, as a function of the nebular density, ρ_0, normalized by that of the minimum mass solar nebula model (Hayashi 1981), ρ_0^H, for the case of $a = 0.1$AU (*solid line*). The nebular temperature and the core accretion rate used are 885K (given by the minimum mass solar nebula model) and $1 \times 10^{-6} M_\oplus \mathrm{yr}^{-1}$, respectively. The result calculated under the assumption of a wholly convective envelope is also shown (*dashed line*).

constant. At $\rho_0 \simeq 10\rho_0^H$, the two lines converge and then the critical core mass decreases as the nebular density increases. At $\rho_0 \simeq 150\rho_0^H$, the critical core mass drops suddenly and afterward decreases with ρ_0 as $M_c^{crit} \propto \rho_0^{-1/2}$; such dependence was analytically predicted by Wuchterl (1993). As seen from this figure, M_c^{crit} is not sensitive to an increase in ρ_0, until the envelope becomes wholly convective.

We can understand the relation between the nebular (i.e., boundary) den-

sity and the critical core mass by comparing two protoplanets with different boundary densities, both the envelopes of which are wholly convective (i.e., the entropy is spatially constant). Suppose that the two protoplanets have the same core mass and the same boundary temperature and, furthermore, that the core mass of the protoplanet with the higher density is the critical core mass. Since the entropy of the envelope is spatially constant, difference in the boundary density leads directly to difference in the entropy of the envelope. The entropy of the protoplanet with the lower boundary density is higher than that of the other protoplanet. Since the higher entropy means that the structure of the envelope is less condensed, it follows that the protoplanet with the lower boundary density have the less massive envelope, that is, its core mass is below the critical core mass. That is the reason why the critical core mass decreases with increasing boundary density.

Figure 8 shows the structures of the envelope when $M_{\rm c} = M_{\rm c}^{\rm crit}$ for typical five ρ_0's. While the outermost region of the envelope is convective even when $\rho_0 = \rho_0^{\rm H}$ (see Eq. (77)), a radiative region develops near $\log T({\rm K}) = 3.3$. As a result, the ρ-T lines converge there in the case where $\rho_0 \leq 5\rho_0^{\rm H}$. This temperature corresponds to the evaporation temperature of silicate grains, $T_{\rm evap}$, and the opacity suddenly becomes small at that point. Thus, the critical nebular density, $\rho_{0,{\rm cr}}^{\rm conv}$, beyond which envelopes are wholly convective, can be found in the following way. The condition for the convective instability is given by Eq. (76). The density at the evaporation point of silicate grains and the nebular density are connected by an adiabat, because the outermost region of the envelope is convective (see Fig. 8):

$$\frac{\rho}{\rho_0} \simeq \left(\frac{T_{\rm evap}}{T_0}\right)^{5/2}, \tag{78}$$

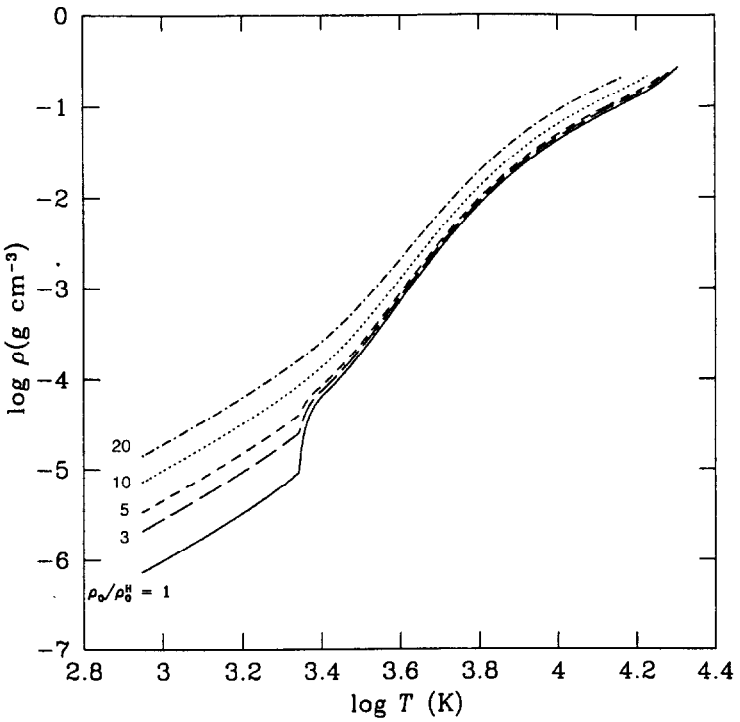

Figure 8: Density and temperature structure of the envelope when $M_c = M_c^{crit}$ for typical five nebular densities. The abscissa and the ordinate are the temperature, T, and the density, ρ, respectively. Each label denotes the nebular density, ρ_0, normalized by that of the minimum mass solar nebula model (Hayashi 1981), ρ_0^H. The nebular temperature and the core accretion rate are the same as those in Fig. 7.

where the polytropic index is assumed to be 5/2. By substituting Eq. (78) into Eq. (76), the critical nebular density for a wholly convective envelope is given by

$$\frac{\rho_{0,cr}^{conv}}{\rho_0^H} \simeq 670 \left(\frac{a}{1AU}\right)^{3/2} \left(\frac{T_0}{T_0^H}\right)^{5/2} \left(\frac{M_c}{20M_\oplus}\right)^{1/3} \left(\frac{\kappa_{evap}}{0.02cm^2g^{-1}}\right)^{-1} \left(\frac{\dot{M}_c}{10^{-6}M_\oplus yr^{-1}}\right)^{-1}, \quad (79)$$

where κ_{evap} is the gas opacity at $T = T_{evap}$. This equation gives $\rho_{0,cr}^{conv}/\rho_0^H \simeq 20$

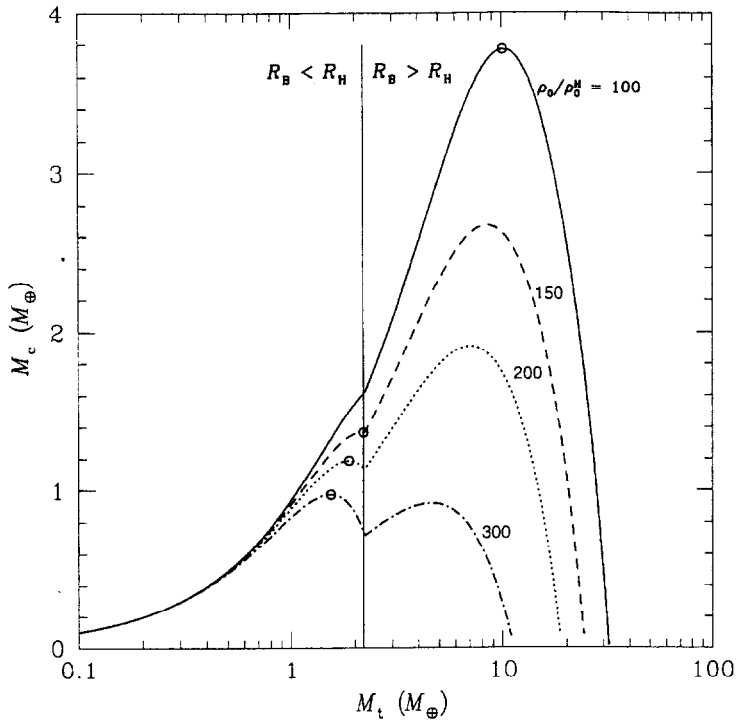

Figure 9: Variation of the core mass (M_c) vs. the total mass (M_t). Each label denotes the nebular density, ρ_0, normalized by that of the minimum mass solar nebula model (Hayashi 1981), ρ_0^H. The open circle $\circ$ denotes the critical core mass, M_c^{crit}, and R_B and R_H mean the Bondi radius and the Hill radius, respectively (see Eq. (8)). The nebular temperature and the core accretion rate are the same as those in Fig. 7.

at 0.1AU, which is consistent with Fig. 7 within a factor of 2.

The sudden drop of M_c^{crit} at $\rho_0 \simeq 150\rho_0^H$ in Fig. 7 can be understood from the behavior of a M_t-M_c curve, which changes with the adopted nebular density. As shown in Fig. 9, the M_t-M_c curve has only one maximum when $\rho_0 = 100\rho_0^H$. Another maximum appears suddenly at lower M_t (i.e., $M_t = 2.2M_\oplus$) when $\rho_0 = 150\rho_0^H$. The total mass of $2.2M_\oplus$ corresponds to that at which the Bondi radius coincides with the Hill radius (see Eq. (10)).

Let us denote the critical core mass and the critical total mass (i.e., the total mass when $M_c = M_c^{crit}$) as $M_c^{crit,B}$ and $M_t^{crit,B}$, respectively, for the case where we define the planetary radius by the Bondi radius, R_B, instead of $\min(R_B, R_H)$ and as $M_c^{crit,H}$ and $M_t^{crit,H}$, respectively, for the case where we define the planetary radius by the Hill radius, R_H. Since the Bondi radius increases faster than the Hill radius as M_t increases (see Eq. (8)), $M_t^{crit,B}$ is always smaller $M_t^{crit,H}$. When $M_t^{crit,B}$ is smaller than the total mass at which $R_B = R_H$, the M_t-M_c curve has two maxima. However, as long as $M_c^{crit,B}$ is less than $M_c^{crit,H}$, the envelope would settle down to a stable structure soon after the envelope begins to contract and captures some amount of the nebular gas, because there exists hydrostatic solutions at the larger M_t where $R = \min(R_B, R_H) = R_H$. In such a case, we should define the critical core mass as the second maximum.

However, the above argument may be meaningless practically, because the nebular density is greater than the critical density for the disk instability (Eq. (7)), whenever the M_t-M_c curve has two maxima. This fact can be analytically proved. As derived by Wuchterl (1993), the critical total mass, M_t^{crit}, for a wholly convective envelope with a constant adiabatic exponent, γ, is given by

$$M_t^{crit} = \sqrt{\frac{1}{12\pi}\frac{3\gamma-4}{(\gamma-1)^4}\left(\frac{c_S^2}{G}\right)^3\frac{1}{\rho_0}}. \tag{80}$$

On the other hand, the total mass at which $R_B = R_H$ is given by Eq. (10). Equating Eq. (80) with Eq. (10), we obtain

$$2\rho_0 H = \frac{\sqrt{2}(3\gamma-4)}{2\gamma(\gamma-1)^4}\frac{c_S\Omega_K}{\pi G}, \tag{81}$$

where H is the density scale height of the disk ($= \sqrt{2}c_S/\gamma\Omega_K$) and $2\rho_0 H$

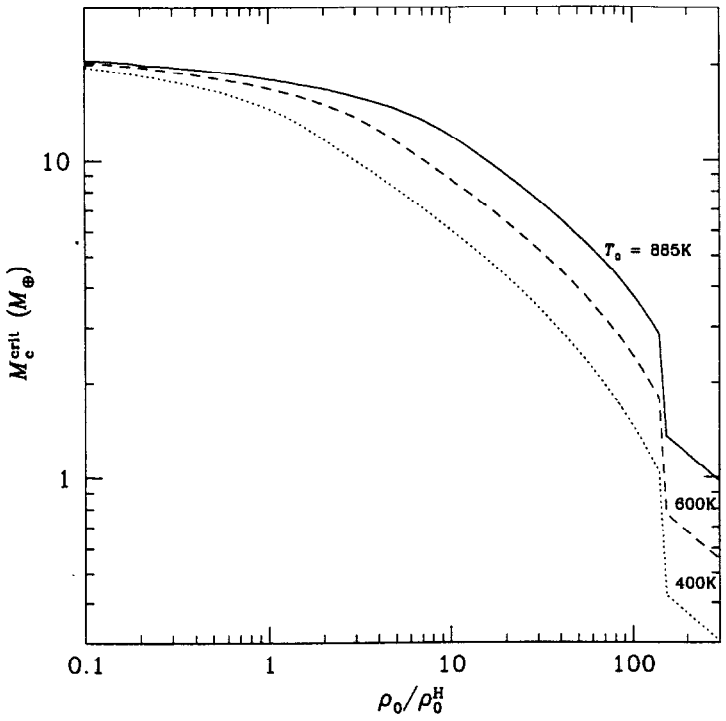

Figure 10: The critical core mass, M_c^{crit}, as a function of the nebular density, ρ_0, normalized by that of the minimum mass solar nebula model (Hayashi 1981), ρ_0^H, for typical three nebular temperatures, 885K (*solid line*), 600K (*dashed line*), and 400K (*dotted line*). The core accretion rate is the same as that in Fig. 7.

means the surface density of the gaseous disk ($= \Sigma_0$). Since the first factor of Eq. (81) gives the order of unity and the last factor means the critical density for the disk instability (see Eq. (6)), this equation indicates that the sudden drop in Fig. 7 corresponds to occurrence of the disk instability and, therefore, the situation expressed by Wuchterl (1993)'s analytical expression for M_c^{crit} can never happen as long as the nebular gas rotates around the central star.

In Fig. 10, the critical core mass is shown as a function of the nebular

density at 0.1AU for typical three nebular temperatures. The temperature of 400K (*dotted line*) corresponds almost to that given by Sasselov and Lecar (2000). As seen from this figure, the critical core mass decreases almost in proportion to the nebular temperature. This is because the lower temperature corresponds to the lower entropy. We can also see that the critical core mass begins to decrease at lower ρ_0 in case of lower T_0. This fact is related to the behavior of $\rho_{0,\mathrm{cr}}^{\mathrm{conv}}$ described in Eq. (79). In the case of $T_0 = 400\mathrm{K}$, which is equal to $0.45T_0^{\mathrm{H}}$ at 0.1AU, $\rho_{0,\mathrm{cr}}^{\mathrm{conv}}$ reduces by about one order of magnitude compared to that for $T_0 = T_0^{\mathrm{H}}$. This means that the convective envelope is readily produced even if $\rho_0 \simeq \rho_0^{\mathrm{H}}$. As a result, the structure of the envelope as well as the critical core mass becomes more sensitive to the outer boundary conditions than those in the case where $T_0 = 885\mathrm{K}$, namely T_0^{H}.

4.2.3 Distance from the Central Star

The nebular density, ρ_0, and temperature, T_0, in general, decrease and the radius of a planet, R, increases with increasing semimajor axis, a (see Eq. (8)). As described above, smaller ρ_0 gives larger critical core mass, whereas smaller T_0 and larger R give smaller critical core mass. Figure 11 shows the critical core mass as a function of $\rho_0/\rho_0^{\mathrm{H}}$ at four typical a's. Each nebular temperature at each semimajor axis is given by Eq. (30). As seen from Fig. 11, when ρ_0 is low (i.e., $\rho_0 \lesssim \rho_0^{\mathrm{H}}$), the critical core mass is almost independent of a and, when $\rho_0 \gtrsim \rho_0^{\mathrm{H}}$, the critical core mass decreases with decreasing a. This indicates that the effect of an increase in ρ_0 with decreasing a is dominant among the above-mentioned three effects in the minimum-mass solar nebula model, where ρ_0^{H} depends strongly on a compared to T_0^{H} and R (see Eqs. (29), (30), and (8)). Furthermore, it can be understood form

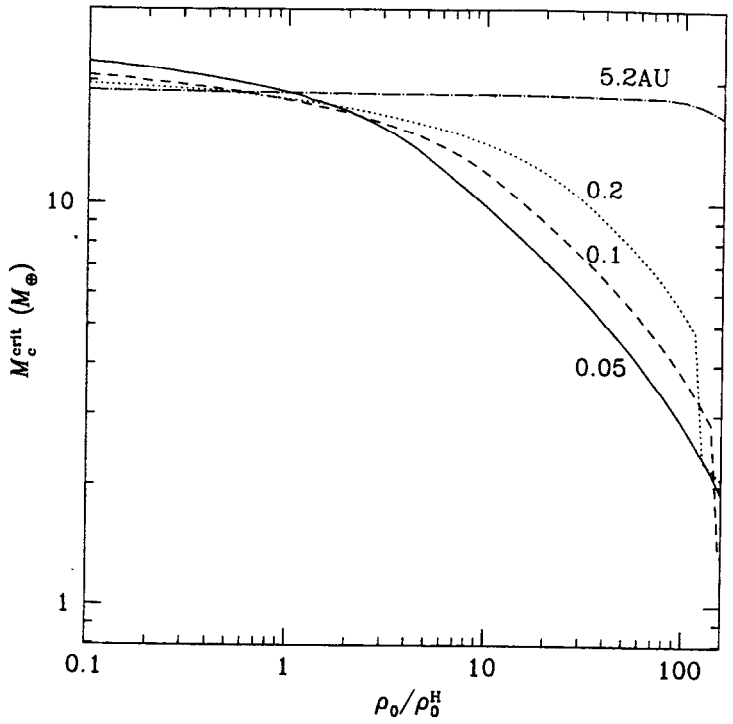

Figure 11: The critical core mass, M_c^{crit}, as a function of the nebular density, ρ_0, normalized by that of the minimum mass solar nebula model (Hayashi 1981), ρ_0^H, for typical four semimajor axes, 0.05AU (*solid line*), 0.1AU (*dashed line*), 0.2AU (*dotted line*), and 5.2AU (*dot-dashed line*). The core accretion rate is the same as that in Fig. 7.

Eq. (79) as well as a brief discussion in the last paragraph of the previous subsection that the normalized density, ρ_0/ρ_0^H, at which the critical core mass begins to decrease, becomes lower, as a decreases.

As also seen in Fig. 11, the critical core mass scarcely depends on the nebular density and does not become small at 5.2AU. When $\rho_0 > \rho_{0,cr}^{conv}$, the critical core mass depends on ρ_0, while a giant planet should not be formed through the nucleated instability when $\rho_0 > \rho_{0,cr}^{disk}$. Therefore, from Eqs. (7) and (79), the region where the critical core mass depends on the nebular

density is given by

$$a \lesssim 0.3\mathrm{AU} \left(\frac{T_0}{T_0^{\mathrm{H}}}\right)^{-10/7} \left(\frac{M_{\mathrm{c}}}{20M_\oplus}\right)^{-4/21} \left(\frac{\kappa_{\mathrm{evap}}}{0.02\mathrm{cm}^2\mathrm{g}^{-1}}\right)^{4/7} \left(\frac{\dot{M}_{\mathrm{c}}}{10^{-6}M_\oplus\mathrm{yr}^{-1}}\right)^{4/7}. \tag{82}$$

That is, at 5.2AU, the critical nebular density for a wholly convective envelope is larger than that for the disk instability and, thus, the critical core mass cannot become small within the practically high nebular density.

For future applications, we should show the dependences of the critical core mass on the boundary conditions of the envelope under the assumption that the envelope is wholly convective. Figure 12 shows the critical core mass as a function of the nebular surface density normalized by that of the minimum-mass solar nebula model, Σ_0^{H}, for typical five semimajor axes. Here we adopt two types of the temperature distributions of the nebula, i.e., $T_0 = 280(a/1\mathrm{AU})^{-1/2}\mathrm{K}$ (Hayashi 1981) and $T_0 = 140(a/1\mathrm{AU})^{-3/7}\mathrm{K}$ (Sasselov and Lecar 2000). In the region we consider, the temperature given by the latter is always lower than that by the former. Therefore, the critical core mass for the latter is smaller than that for the former. Note that the abscissa in Fig. 12 is not the density ρ_0, but the surface density Σ_0, i.e., $2\rho_0 H$.

Let us illustrate how to know the appropriate value of the critical core mass from Fig. 12. We substitute $\dot{M}_{\mathrm{c}}$ and κ_{evap} into Eq. (79) rewriting this equation in terms of $\Sigma_{0,\mathrm{cr}}^{\mathrm{conv}}/\Sigma_0^{\mathrm{H}}$, where $\Sigma_{0,\mathrm{cr}}^{\mathrm{conv}} = 2\rho_{0,\mathrm{cr}}^{\mathrm{conv}} H$. Then, we draw the obtained line supposing that $M_{\mathrm{c}} = M_{\mathrm{c}}^{\mathrm{crit}}$ in Fig. 12. In the domain where $\Sigma_0/\Sigma_0^{\mathrm{H}}$ is larger than this line, this figure gives the critical core mass to be requested. On the other hand, in the domain where $\Sigma_0/\Sigma_0^{\mathrm{H}}$ is smaller than the line, the critical core mass is almost constant and its value is that at the crossover point. Note that the nucleated instability model itself is not valid

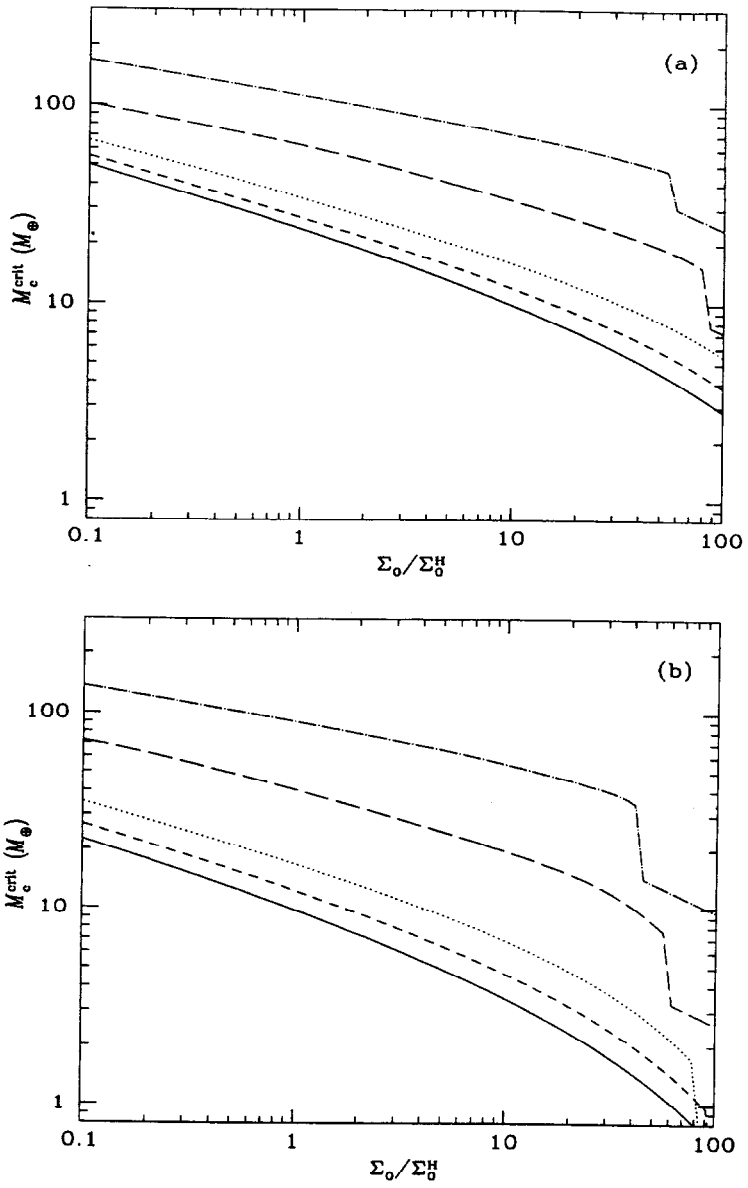

Figure 12: The critical core mass, M_c^{crit}, under the assumption of a wholly convective envelope as a function of the nebular surface density, Σ_0, normalized by that of the minimum mass solar nebula model (Hayashi 1981), Σ_0^H, for typical five semimajor axes, 0.05AU (*solid line*), 0.1AU (*short dashed line*), 0.2AU (*dotted line*), 1.0AU (*long dashed line*), and 5.2AU (*dot-dashed line*). The temperature distribution assumed are of (a) Hayashi (1981) and (b) Sasselov and Lecar (2000).

beyond the density given by Eq. (7).

4.2.4 Summary of Dependences on Properties of the Nebula

Here, we summarize the dependences of the critical core mass on the properties of the nebula:

1. The critical core mass depends on the boundary conditions of the envelope (i.e., the density and temperature of the nebular gas and the distance from the central star), only in the case where the envelope is wholly convective. The envelope does not become wholly convective, until the nebular density becomes as high as that given by Eq. (79).

2. The critical core mass decreases as the nebular density becomes high, the nebular temperature becomes low, and the planetary radius increases. For a given nebular density normalized by that of the minimum mass solar nebula model (Hayashi 1981), the critical core mass decreases as the semimajor axis decreases.

3. For a sufficiently high density, the critical core mass are well expressed by the analytical expression derived by Wuchterl (1993). However, such a density is always larger than the critical density for the disk instability.

5 Discussion and Conclusions

5.1 Summary of This Study

Based on the nucleated instability model, we have investigated the accretion time of the envelope as well as the critical core mass for a wide range of the parameters involved in the accretion process of the envelope. The purpose of our extensive study is to obtain sufficient knowledge in order to discuss quantitatively the formation of the various giant planets (i.e., the giant planets of extrasolar systems as well as those of our solar system).

The parameters are the core accretion rate, the grain opacity, the nebular density and temperature, and the location of a forming protoplanet. The core accretion rate varies considerably depending both on the location and on the formation stage of a protoplanet (see §1.2.1). The grain opacity of the ancient envelope gas is highly uncertain, since it is difficult to know the abundance, sizes, and composition of the grains. In this study, we have used the grain depletion factor, the definition of which is the ratio of the grain opacity in the envelope to that in the interstellar cloud (see §2.4). Finally, the orbital radii of the extrasolar planets range widely from 0.05 to 3 AU. This requires us to investigate the giant planet formation at various locations. Moreover, the observations of nebulae existing around young solar-type stars show a wide range of nebular mass, which we should take into account. The orbital radius and the nebular density and temperature are related to the outer boundary conditions for the envelope.

Before we discuss the formation of the existent giant planets, we summarize our important results that are obtained in the present study.

1. The critical core mass decreases with the core accretion rate and the grain depletion factor. For the sufficiently small values, the critical core mass is as small as about $0.1 M_\oplus$ (§4.1.1). Furthermore, the critical core mass does not depend on the past accretion process of a core (§4.1.2).

2. If the core accretion stops, the considerable accretion of the envelope begins even in the case of a small core ($\gtrsim 0.1 M_\oplus$). However, the accretion time of the envelope increases rapidly as the core mass decreases. The approximate expression of the typical accretion time, $\tau_{\rm g}$, is written as (§4.1.4)

$$\tau_{\rm g} \sim 1 \times 10^{10} f \left(\frac{M_{\rm c}}{M_\oplus} \right)^{-3.5} \ {\rm yr}, \tag{83}$$

where f and $M_{\rm c}$ are the grain depletion factor and the core mass, respectively. The accretion time of the envelope depends very weakly on the past core accretion process.

3. The critical core mass depends on the outer boundary conditions of the envelope only when the envelope is wholly convective (§4.2.1). The critical core mass surrounded by the wholly convective envelope decreases as the nebular density increases, as the nebular temperature decreases, and as the distance from the central star decreases (see §§4.2.2 and 4.2.3). Note that, in that case, the critical core mass does not depend on the core accretion rate and the grain depletion factor.

5.2 Formation of the Giant Planets

We are most interested in the formation time of a giant planet, which we can estimate by calculating both the accretion times of a core and an

envelope. Since both the critical core mass and the accretion time of the envelope beyond the critical core mass scarcely depend on the past core accretion process (see Results 1 and 2), we can consider the two accretion times separately. As described in §1.2.1, a protoplanet (i.e., a solid core) spends most of its formation period in the slow growth stage. We can, therefore, estimate the formation time of the core, $\tau_{\rm c}$, using the equation derived by Tanaka and Ida (1999);

$$\tau_{\rm c} = \begin{cases} 1.8 \times 10^6 \left(\dfrac{M_{\rm trig}}{M_\oplus}\right)^{1/3} \left(\dfrac{\Sigma_{\rm d}}{\Sigma_{\rm d}^{\rm H}}\right)^{-1} \left(\dfrac{a}{1{\rm AU}}\right)^{31/12} & {\rm yr} \quad {\rm for} \ a < 2.7{\rm AU}, \\ 2.7 \times 10^7 \left(\dfrac{M_{\rm trig}}{M_\oplus}\right)^{1/3} \left(\dfrac{\Sigma_{\rm d}}{\Sigma_{\rm d}^{\rm H}}\right)^{-1} \left(\dfrac{a}{5{\rm AU}}\right)^{31/12} & {\rm yr} \quad {\rm for} \ a > 2.7{\rm AU}, \end{cases} \tag{84}$$

where $M_{\rm trig}$ is the mass of the core at which the considerable gas accretion begins (hereafter, called the trigger mass). On the other hand, we can estimate the accretion time of the envelope, $\tau_{\rm env}$, as a function of the trigger mass using Eq. (71). Note that the accretion time, $\tau_{\rm env}$, is about twice as long as the characteristic growth time of the envelope mass, $\tau_{\rm g}$, which was defined in Eq. (67).

If we know the value of the trigger mass, we can calculate both the formation times of the core and the envelope. The trigger mass can be obtained in the following way. The core accretion rate, $\dot{M}_{\rm c}$, is given by (Tanaka and Ida 1999)

$$\dot{M}_{\rm c} = \begin{cases} 1.7 \times 10^{-6} \left(\dfrac{M_{\rm c}}{M_\oplus}\right)^{2/3} \left(\dfrac{\Sigma_{\rm d}}{\Sigma_{\rm d}^{\rm H}}\right) \left(\dfrac{a}{1{\rm AU}}\right)^{-31/12} & M_\oplus {\rm yr}^{-1} \quad {\rm for} \ a < 2.7{\rm AU}, \\ 1.1 \times 10^{-7} \left(\dfrac{M_{\rm c}}{M_\oplus}\right)^{2/3} \left(\dfrac{\Sigma_{\rm d}}{\Sigma_{\rm d}^{\rm H}}\right) \left(\dfrac{a}{5{\rm AU}}\right)^{-31/12} & M_\oplus {\rm yr}^{-1} \quad {\rm for} \ a > 2.7{\rm AU}. \end{cases} \tag{85}$$

Giving a and $\Sigma_{\rm d}$ and substituting them into Eq. (85), we overdraw the

evolutionary path of the core accretion rate on Fig. 2a; the critical core mass, $M_c^{\rm crit}$, is the core mass at which this evolutionary line and the line of the critical core mass cross over. Then, comparing $M_c^{\rm crit}$ with the isolation mass, $M_{\rm iso}$, which is given by Eq. (5), we obtain the trigger mass, $M_{\rm trig}$, i.e., $M_{\rm trig} = \min(M_c^{\rm crit}, M_{\rm iso})$.

The validity of the obtained formation time should be checked on the basis of the observationally inferred lifetime of a nebula, which is of the order of 1×10^7yr (see §1.2.3). As seen from Eq. (84), the core formation time for the typical orbital radius of the extrasolar systems (~ 0.1AU) is about 1×10^4yr even in the case where the trigger mass is $10M_\oplus$; the constraint placed by the nebular lifetime can be easily satisfied. On the other hand, the constraint is a strict one for the giant planets of the solar system, because τ_c is of the order of 1×10^7yr even in the current position of Jupiter. Furthermore, as far as the giant planets of the solar system is concerned, the trigger mass should be in the range of the present core mass inferred by the study of the planetary internal structure.

Before we combine our results with those of the planetary accretion theory, we can find a lower limit of the core mass by comparing Eq. (83) with the nebular lifetime. Since the accretion time of the envelope given by Eq. (83) gives the minimum time required for the giant planet formation, it must be shorter than the nebular lifetime. Under this condition, the lower limits are $\sim 7M_\oplus$, $\sim 4M_\oplus$, and $\sim 2M_\oplus$ for $f = 1$, 0.1, and 0.01, respectively.

5.2.1 Giant Planets of the Solar System

Figures 13a and 13b show, respectively, the trigger mass and the formation time, $\tau_{\rm form}$ $(= \tau_c + \tau_{\rm env})$, of Jupiter (i.e., $a = 5.2$AU) as functions of

Σ_d/Σ_d^H for five values of the grain depletion factor, f. As seen from Fig. 13a, in the case of relatively low surface density (for example, $\Sigma_d/\Sigma_d^H < 6$ for the case of $f = 1$), M_{trig} is equal to M_{iso}, which increases with Σ_d/Σ_d^H (i.e., $M_{iso} \propto \Sigma_d^{3/2}$), and does not depend on f. On the other hand, in the case of large Σ_d, $M_{trig} = M_c^{crit}$. Hence, M_{trig} depends on f but only weakly on Σ_d/Σ_d^H (M_c^{crit} depending on Σ_d/Σ_d^H through $\dot{M}_c$; $M_c^{crit} \propto \dot{M}_c^{0.3}$).

As seen from Fig. 13b, in the case of the minimum-mass solar nebula (i.e., $\Sigma_d/\Sigma_d^H = 1$), τ_{form} deceases greatly as f decreases. This is because τ_{env} (i.e., τ_g) decreases in proportion with decreasing f (see Eq. (83)). The formation time, τ_{form}, also decreases with increasing Σ_d/Σ_d^H. In the case where $\Sigma_d/\Sigma_d^H \lesssim 3$ and $f \geq 0.1$, $\tau_{form} \simeq \tau_{env}$. In this case, since M_{iso} increases with Σ_d/Σ_d^H and τ_{env} (i.e., τ_g) decreases rapidly with increasing M_{iso} (see Eq. (83)), τ_{form} decreases rapidly as Σ_d/Σ_d^H increases. On the other hand, in the case where $\Sigma_d/\Sigma_d^H \gtrsim 3$ or $f \leq 0.01$, $\tau_{form} \simeq \tau_c$. In such case, since the dependence of τ_c on M_{trig} is small (see Eq. (84)) compared to that of τ_{env}, τ_{form} decreases only slowly with increasing Σ_d/Σ_d^H.

From Fig. 13b, we can find that, if $f \leq 0.01$, Jupiter can be formed in the period of the order of 1×10^7yr (i.e., the nebular lifetime) even in the case of the minimum-mass solar nebula. Even if f is larger than 0.01, Jupiter can be formed in the nebula with surface density a few times as high as that of the minimum-mass solar nebula. In those cases, the trigger masses are 2 to $9M_\oplus$ as seen from Fig. 13a. These values are consistent with the present core mass of Jupiter inferred from the study of the internal structures of the giant planets (i.e., $0 - 10M_\oplus$).

In the case of Saturn (see Figs. 14a and b), the situation may be severe.

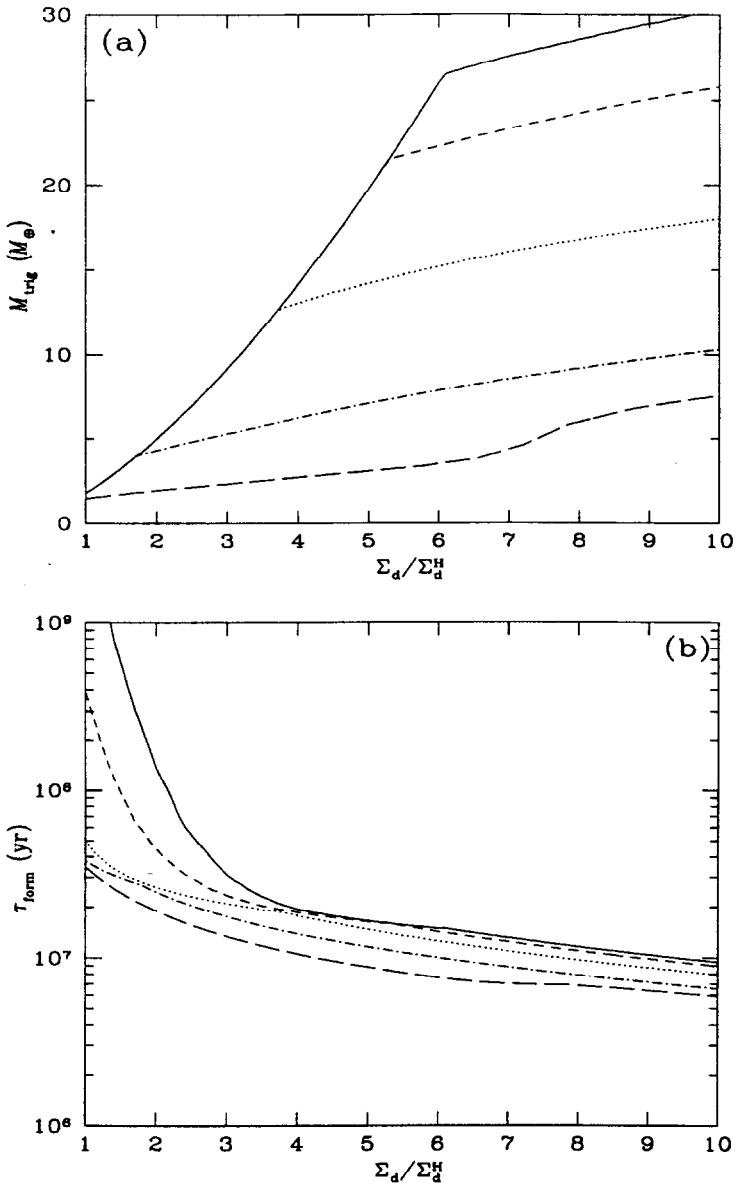

Figure 13: The trigger mass, $M_{\rm trig}$, (Fig. (a)) and the formation time (i.e., the sum of the accretion times of the core and the envelope), $\tau_{\rm form}$, of Jupiter (Fig. (b)) as functions of the surface density of solid materials, $\Sigma_{\rm d}$, normalized by that of the minimum-mass solar nebula, $\Sigma_{\rm d}^{\rm H}$, for $f = 1$ (*solid line*), 1×10^{-1} (*short dashed line*), 1×10^{-2} (*dotted line*), 1×10^{-3} (*dot-dashed line*), 1×10^{-4} (*long dashed line*).

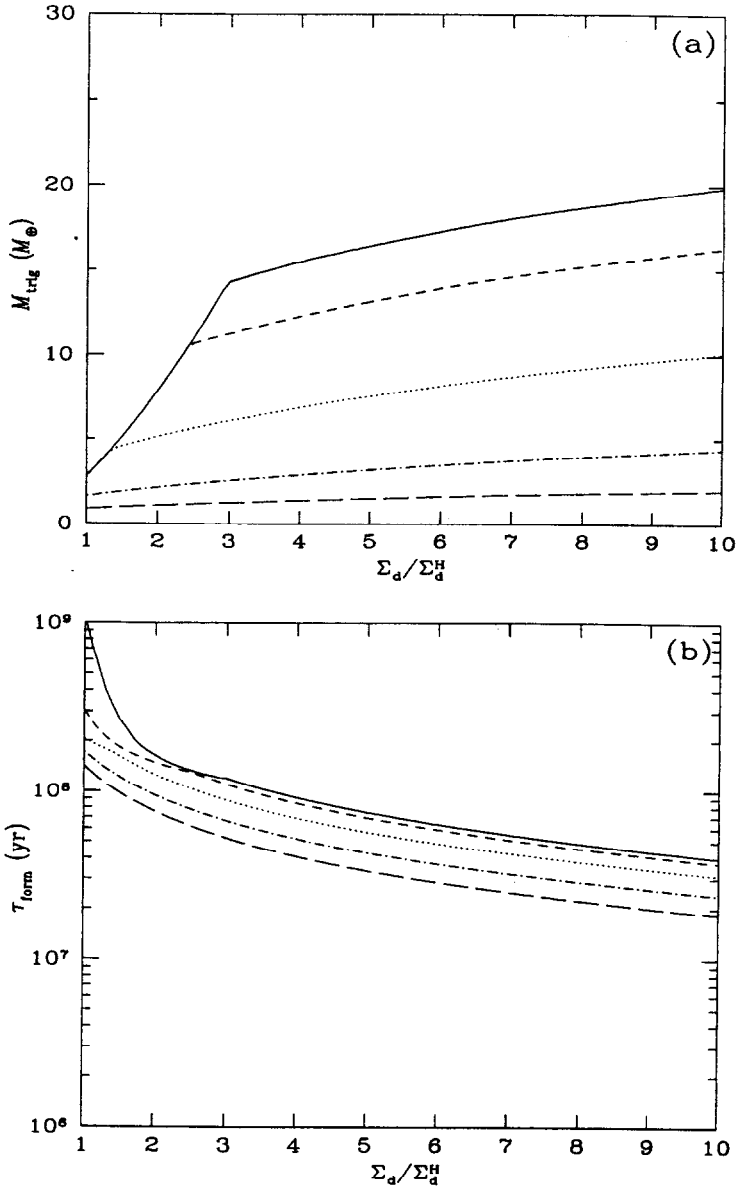

Figure 14: The trigger mass, $M_{\rm trig}$, (Fig. (a)) and the formation time (i.e., the sum of the accretion times of the core and the envelope), $\tau_{\rm form}$, of Saturn (Fig. (b)) as functions of the surface density of solid materials, $\Sigma_{\rm d}$, normalized by that of the minimum-mass solar nebula, $\Sigma_{\rm d}^{\rm H}$, for $f = 1$ (*solid line*), 1×10^{-1} (*short dashed line*), 1×10^{-2} (*dotted line*), 1×10^{-3} (*dot-dashed line*), 1×10^{-4} (*long dashed line*).

In the minimum-mass solar nebula, $\tau_{\rm form}$ is longer than 1×10^8yr even if very small f ($< 1 \times 10^{-4}$) is considered. Furthermore, even if f is very small, very large surface densities are required, compared to $\Sigma_{\rm d}$; for example, $\Sigma_{\rm d} \gtrsim 5\Sigma_{\rm d}^{\rm H}$ and $f < 1 \times 10^{-3}$ are needed for the formation within 5×10^7yr. In the case of Neptune and Uranus, the situations are extremely severe, because, even if the lifetime of the nebula was 1×10^8yr, $\Sigma_{\rm d} > 10\Sigma_{\rm d}^{\rm H}$ would be required. It is very difficult to explain how the solar system lost such a large amount of solid materials.

Such difficulty arises apparently from the quite long accretion time of the core, namely the strong dependence on the distance from the Sun, a (see Eq. (84)). It may be inevitable to consider that the planetary cores formed around the current location of Jupiter and then each of them moved outwards to each present position. After Jupiter had been formed, its gravitational effect would be important to the protoplanets around it. As described in §1.2.1, several protoplanets form with the orbital separations of about 10 times as large as their tidal radii owing to orbital repulsion (Kokubo and Ida 1998). That is, several protoplanets with a few $M_\oplus$ would form around 5AU. A protoplanet, the mass of which reached the isolation mass fastest, could become Jupiter and other protoplanets with somewhat larger semimajor axes may be thrown far away by the massive planet. The distance of 10 times as great as the tidal radius of Jupiter is about 5AU, which is consistent with the present separation between Jupiter and Saturn. A migrated protoplanet would capture the nebular gas in the new location. Such a process would occur successively to form Uranus and Neptune (also see Thommes *et al.* (1999) and Bryden *et al.* (2000)). The relatively small envelope masses of

Uranus and Neptune (1 to $4M_\oplus$) may be explained if we consider that such a process occurred on the way of the dissipation of the nebular gas, because proto-Uranus and Neptune with small cores would experience the phases of a moderate increase in the envelope mass and could not experience the rapid gas accretion era, which was also pointed by Pollack *et al.* (1996).

5.2.2 Giant Planets of Extrasolar Systems

The in situ formation of the extrasolar giant planets, which orbit very close to their parent stars (0.05 to 3AU), was considered to be very difficult because of small isolation mass (see Eq. (5)). For this reason, some previous workers (Papaloizou and Terquem 1999; Bodenheimer *et al.* 2000) considered the ways in which large cores ($> 10M_\oplus$) are formed. In contrast, we propose the cases in which a $2-3M_\oplus$ core can capture a large amount of the nebular gas at 0.05AU. The point is to consider the formation in the dense nebula whose mass is about 10 times as large as that of the minimum-mass solar nebula; such a nebula has already been detected, as described in §1.2.4.

If a core becomes isolated from planetesimals completely when its mass becomes larger than $2M_\oplus$, it can capture a large amount of the nebular gas in the period comparable to the nebular lifetime in the case of $f \lesssim 0.01$ (see Eq. (83)). Even if the core does not become isolated, the critical core mass is as small as $2-3M_\oplus$ in such a dense nebula, although the nebula have to be a passive one like that given by Sasselov and Lecar (2000) (see Fig. 12b). In this case, the condition that grains are highly depleted in the planet-forming nebula can be eliminated and, nevertheless, the formation time is quite short. The accretion time of a solid core is very short at 0.05AU mainly because of the short Keplerian time. For example, the simple estimation by Tanaka

and Ida (1999) gives about 100yr for a core to grow to $3M_\oplus$. Note that such estimation may be over-optimistic, since the core could vaporize if it was formed in such a short period. In that case, cooling of the vaporized gas regulates the formation of the core. The cooling time, $\tau_{\rm cool}$, is given approximately by

$$\tau_{\rm cool} \sim \frac{CTM_{\rm c}}{4\pi R^2 \sigma_{\rm SB}(T^4 - T_0^4)}, \tag{86}$$

where C is the heat capacity of the vaporized gas. Putting $C = 1 \times 10^8 {\rm erg/K}$ (i.e., a typical value for the perfect gas), $M_{\rm c} = 3M_\oplus$, $R > 1 \times 10^9 {\rm cm} (\sim {\rm r_c})$, $T = 2000{\rm K}$ (i.e., typical condensation temperature of silicate), and $T_0 = 1250{\rm K} (= T_0^{\rm H})$, we have $\tau_{\rm cool} \lesssim 1 \times 10^4 {\rm yr}$.

On the other hand, the gas accretion time is also short, since the considerable luminosity is radiated from the envelope when the core mass is the critical core mass. The accretion time of the envelope is given by Eq. (71), which can be written as $M_{\rm c}^{\rm crit}/\dot{M}_{\rm c}$ on the order of magnitude with the use of the relation, $L^{\rm crit} \simeq GM_{\rm c}^{\rm crit}\dot{M}_{\rm c}/r_{\rm c}$. Even if low $\dot{M}_{\rm c}$ of $1 \times 10^{-5} M_\oplus {\rm yr}^{-1}$ is assumed, the accretion time of the envelope is $\sim 1 \times 10^5 {\rm yr}$ for the accretion time of an gaseous envelope. Thus, the total accretion time is very short compared to the typical lifetime of the nebula ($1 \times 10^7 {\rm yr}$).

The isolation mass given by Eq. (5) is about $1M_\oplus$, that is, is somewhat smaller than the required core mass. We can, however, consider the possibilities that the surface density was somewhat higher than that given by the surface density distribution of the minimum-mass solar nebula originally or because of inflow of solid materials on the central star.

To confirm such a formation scenarios of the giant planets close to the central stars mentioned above, there still remain problems to be solved. The

most serious problem is how large amount of gas a planet can capture. No further accretion of gas is considered to occur, when the width of a gap around a planet becomes larger than the local scale height of a disk (Lin and Papaloizou 1993). The scale height of the disk is so small around 0.05AU that the final mass would be very small compared to Joupiter's mass. However, the width of the gap depends on the uncertain parameter of the disk, i.e., the effective viscosity that may be produced by turbulence or a magnetic force. Thus, the issue of the limiting mass of a giant planet is still controversial. In this sense, it is still an open problem whether the detected extrasolar planets very close to the central stars could form in their current positions.

Acknowledgements

The author wishes to express his gratitude to Professor K. Nakazawa for a great deal of valuable advice and the critical reading of this manuscript. He is deeply indebted to Dr. H. Emori for helpful advice and fruitful discussions. He is also grateful to Assistant Professor S. Ida and Dr. H. Tanaka for fruitful discussions. He thanks D. Saumon for giving EOS data and D. Alexander for opacity data. He also thanks Ms. K. Kudo for continuing encouragement. This work has been supported, in part, by Research Fellowships of the Japan Society for the Promotion of Science for Young Scientists (No. 10107) and by Grant-in-Aid for Specially Promoted Research (No. 11101002).

References

ALEXANDER, D. R., AND FERGUSON, J. W. 1994, Low-temperature Rosseland opacities. *Astrophys. J.*, **437**, 879

BECKWITH, S. V. W., AND SARGENT, A. I. 1996, Circumstellar disks and the search for neighbouring planetary systems. *Nature*, **383**, 139

BODENHEIMER, P., AND POLLACK, J. B. 1986, Calculations of the accretion and evolution of giant planets: the effects of solid cores. *Icarus*, **67**, 391

BODENHEIMER, P., HUBICKYJ, O., AND LISSAUER, J. J. 2000, Models of the in situ formation of detected extrasolar giant planets. *Icarus*, **143**, 2

BÖHM-VITENSE, E. 1958, Über die wasserstoffkonvektionszone in sternen verschiedener effektivtemperaturen und leuchtkräfte. Mit 5 textabbildungen. *Z. Astrophys.*, **46**, 108

BRYDEN, G., LIN, D. N. C., AND IDA, S. 2000, Protoplanetary formation. I. Neptune. *Astrophys. J.*, **544**, 481

CHIANG, E. I., AND GOLDREICH, P. 1997, Spectral energy distributions of T Tauri stars with passive circumstellar disks. *Astrophys. J.*, **490**, 368

CUZZI, J. N., DOBROVOLSKIS, A. R., AND CHAMPNEY, J. M. 1993, Particle-gas dynamics in the midplane of a protoplanetary nebula. *Icarus*, **106**, 102

GOLDREICH, P., AND WARD, W. R. 1973, The formation of planetesimals. *Astrophys. J.*, **183**, 1051

GREENBERG, R., HARTMAN, W. K., CHAPMAN, C. R., AND WACKER,

J. 1978, Planetesimals to planets - numerical simulation of collisional evolution. *Icarus*, **35**, 1

GREENZWEIG, Y., AND LISSAUER, J. J. 1992, Accretion rates of protoplanets. II - Gaussian distributions of planetesimal velocities. *Icarus*, **100**, 440

HAYASHI, C. 1981, Structure of the solar nebula, growth and decay of magnetic fields and effects of magnetic and turbulent viscosities on the nebula. *Prog. Theor. Phys. Suppl.*, **70**, 35

HAYASHI, C., NAKAZAWA, K., AND NAKAGAWA, Y. 1985, Formation of the solar system. in *Protostars & Planets II*, ed. D. C. Black and M. S. Matthews (Tucson: Univ. Arizona Press), 1100

HENYEY, L. G., FORBES, J. E., AND GOULD, N. L. 1964, A new method of automatic computation of stellar evolution. *Astrophys. J.*, **139**, 306

IDA, S., AND MAKINO, J. 1993, Scattering of planetesimals by a protoplanet - slowing down of runaway growth. *Icarus*, **106**, 210

IKOMA, M. 1998, Formation of the proto-giant planets: onset of the gravitational instability of the protoplanetary atmosphere and the rate of planetesimals accretion. master thesis, Tokyo Institute of Technology

IKOMA, M., EMORI, H., AND NAKAZAWA, K. 1998, Formation of a proto-Jovian envelope for various planetary accretion rates. *J. Phys.: Condens. Matter*, **10**, 11537

IKOMA, M., NAKAZAWA, K., AND EMORI, H. 2000, Formation of giant planets: dependences on core accretion rate and grain opacity. *Astrophys. J.*, **537**, 1013

KIPPENHAHN, R., WEIGERT, A., AND HOFMEISTER, E. 1967, Methods for calculating stellar evolution. *Methods In Computation Physics*, **7**, 129

KIPPENHAHN, R., AND WEIGERT, A. 1990, *Stellar Structure and Evolution* (New York: Springer-Verlag)

KOKUBO, E., AND IDA, S. 1998, Oligarchic growth of protoplanets. *Icarus*, **131**, 171

LIN, D. N. C., AND PAPALOIZOU, J. C. B. 1993, On the tidal interaction between protostellar disks and companions. in *Protostars and Planets III*, ed. E. H. Levy and J. Lunine (Tucson: Univ. Arizona Press), 749

MARCY, G. W., AND BUTLER, R. P. 1998, Detection of extrasolar giant planets. *Annu. Rev. Astron. Astrophys.*, **36**, 57

MAYOR, M., AND QUELOZ, D. 1995, A Jupiter-mass companion to a solar-type star. *Nature*, **378**, 355

MIKI, S. 1982, The gaseous flow around a protoplanet in the primitive solar nebula. *Prog. Theor. Phys.*, **67**, 1053

MIYOSHI, K., IKOMA, M., EMORI, H., AND NAKAZAWA, K. 1996, The stability of the envelope of proto-Jovian planets. *Proc. 29th ISAS Lunar Planet. Symp.*, , 185

MIZUNO, H., NAKAZAWA, K., AND HAYASHI, C. 1978, Instability of a gaseous envelope surrounding a planetary core and formation of giant planets. *Prog. Theor. Phys.*, **60**, 699

MIZUNO, H. 1980, Formation of the giant planets. *Prog. Theor. Phys.*, **64**, 544

PAPALOIZOU, J. C. B., AND TERQUEM, C. 1999, Critical protoplanetary

core masses in protoplanetary disks and the formation of short-period giant planets. *Astrophys. J.*, **521**, 823

PERRI, F., AND CAMERON, A. G. W. 1974, Hydrodynamic instability of the solar nebula in the presence of a planetary core. *Icarus*, **22**, 416

POLLACK, J. B., MCKAY, C. P., AND CHRISTOFFERSON, B. M. 1985, A calculation of the Rosseland mean opacity of dust grains in primordial solar system nebulae. *Icarus*, **64**, 471

POLLACK, J. B., HUBICKYJ, O., BODENHEIMER, P., LISSAUER, J. J., PODOLAK, M., AND GREENZWEIG, Y. 1996, Formation of the giant planets by concurrent accretion of solids and gas. *Icarus*, **124**, 62

SAFRONOV, V. S. 1969, *Evolution of the Protoplanetary Cloud and Formation of the Earth and Planet.* (Moscow: Nauka Press)

SASSELOV, D. D., AND LECAR, M. 2000, On the snow line in dusty protoplanetary disks. *Astrophys. J.*, **528**, 995

SAUMON, D., CHABRIER, G., AND VAN HORN, H. M. 1995, An equation of state for low-mass stars and giant planets. *Astrophys. J. Suppl.*, **99**, 713

SEKIYA, M. 1983, Gravitational instabilities in a dust-gas layer and formation of planetesimals in the solar nebula. *Prog. Theor. Phys.*, **69**, 1116

SHU, F. 1991, *The Physics of Astrophysics, Vol. I. Radiation* (Mill Valley: University Science Books)

STEVENSON, D. J. 1982a, Interiors of the giant planets. *Annu. Rev. Earth Planet. Sci.*, **10**, 257

STEVENSON, D. J. 1982b, Formation of the giant planets. *Planet. Space*

Sci., **30**, 755

STROM, S. E., EDWARDS, S., AND SKRUTSKIE, M. F. 1993, Evolutionary timescales for circumstellar disks associated with intermediate- and solar-type stars. in *Protostars and Planets III*, ed. E. H. Levy and J. I. Lunine (Tucson: Univ. Arizona Press), 837

TANAKA, H., AND IDA, S. 1999, Growth of a migrating protoplanet. *Icarus*, **139**, 350

TAJIMA, N., AND NAKAGAWA, Y. 1997, Evolution and dynamical stability of the proto-giant-planet envelope. *Icarus*, **126**, 282

THI, W. F., BLAKE, G. A., VAN DISHOECK, E. F., VAN ZADELHOFF, G. J., HORN, J. M. M., BECKLIN, E. E., MANNINGS, V., SARGENT, A. I., VAN DEN ANCKER, M.E., AND NATTA, A. 2001, Substantial reservoirs of molecular hydrogen in the debris disks around young stars. *Nature*, **409**, 60

THOMMES, E. W., DUNCAN, M. J., AND LEVISON, H. F. 1999, The formation of Uranus and Neptune in the Jupiter-Saturn region of the Solar System. *Nature*, **402**, 635

TOOMRE, A. 1964, On the gravitational stability of a disk of stars. *Astrophys. J.*, **139**, 1217

WARD, W. R. 1997, Protoplanet migration by nebula tides. *Icarus*, **126**, 261

WEIDENSCHILLING, S. J. 1980, Dust to planetesimals - settling and coagulation in the solar nebula. *Icarus*, **44**, 172

WETHERILL, G. W., AND STEWART, G. R. 1989, Accumulation of a swarm of small planetesimals. *Icarus*, **77**, 330

WUCHTERL, G. 1991, Hydrodynamics of giant planet formation. III. Jupiter's nucleated instability. *Icarus*, **91**, 53

WUCHTERL, G. 1993, The critical mass for protoplanets revisited - massive envelopes through convection. *Icarus*, **106**, 323

WUCHTERL, G. 1995, Giant planet formation. *Earth, Moon, and Planets*, **67**, 51

WUCHTERL, G., GUILLOT, T., AND LISSAUER, J. J. 2000, Giant planet formation. in *Protostars and Planets IV*, ed. V. Mannings, A. P. Boss, and S. S. Russell (Tucson: Univ. Arizona Press), 1081

ZUCKERMAN, B., FORVEILLE, T., AND KASTNER, J. H. 1995, Inhibition of giant planet formation by rapid gas depletion around young stars. *Nature*, **373**, 494